The Photophysics and Dynamics of Diphenylbutadiene in Alkane and Perfluoroalkane Solvents

K. Dahl, R. Biswas,[†] and M. Maroncelli*

Department of Chemistry, The Pennsylvania State University, 152 Davey Laboratory, University Park, Pennsylvania 16802

Received: January 17, 2003; In Final Form: April 29, 2003

Absorption and emission spectral characteristics, quantum yields, radiative and nonradiative rates, and rotation times of *trans,trans*-1,4-diphenyl-1,3-butadiene (DPB) in perfluoroalkane and alkane solvents are reported. The emission spectra and radiative rates show a continuous change in the character of the emitting state of DPB with solvent polarizability, presumably due to solvent-induced changes in the relative energies of the $2A_g$ and $1B_u$ states. Rotation times measured in these nonpolar solvents do not conform to any available theory of rotational friction; however, deviations from hydrodynamic predictions can be roughly correlated with the solute/solvent size ratio. Nonradiative decay rates are assumed to reflect an adiabatic trans−cis isomerization process. The rates measured here, together with collected literature data in alkane and alcohol solvents, are analyzed using a Kramers' barrier crossing model coupled to a simple dielectric description of how the reactive potential varies with solvent. By using estimates of friction obtained from rotation times, we can reasonably model the data in all solvents if it is assumed that the scaling between reactive friction and rotational friction (ζ/ζ_{rot}) differs among the various solvent classes: alkanes (ζ/ζ_{rot}) $\approx$ 1, perfluoroalkanes (ζ/ζ_{rot}) $\approx$ 0.2, and *n*-alcohols (ζ/ζ_{rot}) $\approx$ 0.4

I. Introduction

In this paper we report new results on the photophysical properties and the rotation and isomerization rates of *trans,trans*-1,4-diphenylbutadiene (DPB) in perfluoroalkane and alkane solvents. The original motivation for this work derived from an interest in the unusual nature of perfluoroalkane−hydrocarbon interactions. Beginning in the early 1950s when perfluoroalkane solvents first became readily available, their distinctive character, especially with regard to interactions with alkanes and aromatic hydrocarbons, has been recognized.[1,2] A variety of thermodynamic data reveals that the interactions between perfluoroalkanes and alkanes are weaker than anticipated based on their pure component properties. Despite decades' worth of speculation, this behavior has yet to be completely explained.[3] The fact that aromatic hydrocarbons interact very weakly with perfluorinated solvents has also long been known from observations of electronic spectra, which, in perfluorinated solvents, are often quite similar in appearance to gas-phase spectra.[4,5] To some extent, gas-like spectra are expected on the basis of the very low dielectric constants of perfluorinated solvents; however, spectral shifts of aromatic solutes in perfluorinated solvents depart markedly from the dielectric correlations established in all other types of solvents.[6,7] This departure has also eluded satisfactory explanation.

The initial goal of this study was to determine whether such weak hydrocarbon−perfluorocarbon interactions also lead to anomalous frictional forces in perfluoroalkane solvents. Because we had been working with DPB in other contexts,[8,9] we decided to use its rotation and isomerization rates as probes of friction in perfluoroalkane solvents. As a guide to "normal" behavior we also measured these same rates in alkane solvents. Unfortunately, our results are not definitive with regard to the question of whether friction is anomalous in perfluoroalkane solvents. Rotation data tend to say no, isomerization data, yes. Both sets of data mainly serve to underscore how poor our quantitative understanding of friction is, even in "normal" solvents. However, as a result of this investigation we have uncovered a number of new features of the photophysics of DPB and its solvent dependence. We have also attempted to analyze the data collected here together with accumulated literature data to form a more global picture of how the isomerization of DPB varies with solvent. These latter results form the main topics of the present report.

DPB has already been the subject of numerous investigations. Beginning with the pioneering measurements of Fleming and co-workers[10−12] a number of groups, especially those of Troe[13−18] and Kauffman,[19−23] have used the excited-state isomerization of DPB as a model for understanding frictional effects on chemical reactions.[24−28] Many workers have also addressed the nature of the excited-states of DPB in relation to the other members of the diphenylpolyene series.[29−35] A valuable overview of much of this work prior to 1990 was provided in the thorough review by Saltiel and Sun.[36]

Although a great deal is known from prior research, some nontrivial questions about the photophysics of DPB remain. Virtually all studies of DPB as a model reaction simply assume that its fast nonradiative decay reflects an adiabatic trans−cis isomerization process, comparable to the reaction of its even more extensively studied cousin, stilbene.[37,38] Such a picture is reasonable, and indeed it is this viewpoint we will adopt here. Nevertheless, it is important to appreciate how little is actually known about the potential surface on which this reaction is presumed to occur. First, as noted in several reviews[36,39] (but

* Corresponding author. E-mail: mpm@chem.psu.edu. Phone: (814) 865-0898. Fax: (814) 863-5319.

[†] Currently at the S.N. Bose National Centre for Basic Sciences, Salt Lake, Kolkata, India.

10.1021/jp0300703 CCC: $25.00
Published on Web 07/03/2003

ignored elsewhere) the quantum yields for photoproduction of cis−trans DPB from trans−trans reactant are much smaller[40,41] than in stilbene and its derivatives.[38] This observation implies either that the topography of the S_1 surface has a different relationship to that of S_0 in DPB compared to stilbene or that internal conversion processes other than isomerization are operative in DPB.

Another potential complication is the fact that the two states, $2A_g$ and $1B_u$, presumed responsible for producing the S_1 surface are nearly degenerate in DPB. In the gas phase, the $2A_g$ state is the lowest excited singlet state, and low-energy excitation of jet-cooled samples produces emission mainly having the character of the 1-photon forbidden $2A_g$ state.[26,29,31] Radiative rate measurements show that this $2A_g$ emission borrows significant intensity from the allowed $1B_u$ state, which lies $\sim$1000 cm^{-1} higher in energy.[27] An interesting aspect of these jet studies is the unexplained coincidence of the $1B_u$ origin and the threshold for the fast nonradiative decay attributed to isomerization. In thermalized gases near room temperature, the emission of DPB can be interpreted as arising primarily from levels of the $1B_u$ state in thermal equilibrium with the $2A_g$ state.[31] In solution, the state ordering is not known with certainty. Assuming that both of these states in DPB display solvent sensitivities similar to those of diphenylhexatriene,[42] it has been suggested[32] that the origins of the two states cross in solvents of very low polarizability (like perfluoroalkanes) such that the $1B_u$ state is the lowest state in most solvents. Whatever the order, it is clear that $2A_g$ and $1B_u$ are nearly degenerate in solution. Resonance Raman studies suggest that S_1 is best viewed as a strongly mixed combination of these two nominal states.[33,34] How an energy barrier is produced by interactions between two nearly isoenergetic states or what other states might be involved in producing the reactive barrier remain open questions.[39] Finally, although an early report[43] that nonadiabatic transitions between states play an important role in the photodynamics of DPB has since been discredited,[28] one still wonders whether a purely adiabatic description of the DPB reaction is appropriate given the proximity of the $2A_g$ and $1B_u$ states in solution.

The work reported here bears on at least some of the above issues. Careful examination of the emission line shapes (section III.A) and radiative rates (section III.B) provides clear evidence of a systematic variation in the character of the emitting state of DPB with solvent polarizability. Presumably this variation reflects changes in $2A_g-1B_u$ mixing as the energy gap between these states varies with solvent. (The use of perfluoroalkane solvents renders this previously unnoticed behavior particularly evident.) We find no evidence that this variation in the $2A_g/1B_u$ character is of direct relevance to the excited state reaction of DPB. Thus, although the nonradiative rates of DPB in perfluoroalkane and alkane solvents differ substantially ($\sim$5-fold), these differences appear to result primarily from the distinct frictional characteristics of these solvents, rather than from differences in the reactive potential. The apparent barrier to reaction does change with solvent, but such changes are only obvious when a wider range of solvent polarities is considered. We have analyzed the data collected here together with the considerable body of data available on the reaction of DPB in alkane and alcohol solvents by using a Kramers' barrier crossing model coupled to a simple dielectric description of the solvent dependence of the reactive potential (section III.D). Using rotation times of DPB to empirically measure solvent friction (section III.C), we find that all of these data can be correlated with reasonable accuracy if one allows for different scaling factors relating rotational and reactive friction in different solvent classes. The reasonableness of such a treatment and its implications are discussed in section IV.

II. Experimental Methods

The DPB (*trans*,*trans*-1,4-diphenyl-1,3-butadiene; 98%) used for most of the measurements reported here was purchased from Aldrich and recrystallized three times from hexane. No impurities were detected by either TLC or NMR measurements. The *n*-alkane solvents were spectrophotometric grade (99+%), and were typically used as received from Aldrich. Perfluorinated solvents were purchased from Lancaster Synthesis: perfluoro-*n*-heptane (98%), perfluoro-*n*-octane (98%), perfluoro-*n*-nonane (99%), perfluoro(decahydronaphthalene) (95%), perfluorotributylamine (94%), perfluoro(methylcyclohexane) (95%), and perfluorohexanes (98%). Most of these solvents were also used as received. *n*-Pentane, *n*-hexane, cyclohexane, and perfluoro-*n*-pentane were distilled under argon prior to use. After distillation, all solvents were spectroscopically clean in the areas of interest.

Individual samples were prepared in standard 1 cm quartz cuvettes to have an optical density of <0.08 at the excitation wavelength and were bubbled under dry argon or nitrogen for 15 min to remove dissolved oxygen. This bubbling was mainly precautionary as any effects of oxygen were found to be minor. Samples above -5 °C were thermostated to ±0.1 °C by using a circulating water bath and sample-holder assembly. Low-temperature samples utilized a liquid nitrogen cryostat (Oxford ITC4). The latter samples were held in a special vacuum-tight "cryocuvette" (NSG) and were temperature controlled to within ±0.1 °C. All time-resolved samples employed excitation filters on the two cuvette faces away from the excitation/emission directions. This practice has been found to reduce the effect of reflections in the time-resolved decays, which leads to improved fitting.

Steady-state absorption measurements were carried out on a Hitachi U-3000 UV−vis spectrophotometer, with a resolution of 2 nm, against a solvent blank. Steady-state emission was collected with a Spex Fluorolog 212 fluorimeter with a resolution of 2 nm. Emission was excited near the peak of the absorption spectrum; however, no wavelength dependence was noted in any of the solvents examined. The F212 incorporates a quantum counter to correct for lamp fluctuations and has been corrected for instrumental emission wavelength dependence. Solvent blanks were subtracted from the emission to correct for any solvent background. (Solvent blanks were not utilized for samples run in the cryostat; however, the background in these cases was $<10^{-3}$ of the overall emission intensity, and therefore, its effects are expected to be virtually negligible.)

Fluorescence quantum yields Φ_{fl} were determined relative to a reference solution of quinine sulfate dihydrate in 0.5 M H_2SO_4 ($\Phi_R = 0.546$[44,45]) according to standard procedures[44,46] using the relation

$$\Phi_{fl} = \frac{n_R^2 I_S (1 - 10^{-0.5A_R})}{n_S^2 I_R (1 - 10^{-0.5A_S})} \Phi_R \qquad (1)$$

where n_X is the refractive index, I_X the integrated emission photon intensity, and A_X the absorbance of the sample (X = S) and reference (X = R) solutions. Initial attempts to measure quantum yields were hampered by noticeable photodegradation of solution-phase DPB samples under the high-intensity Xe arc lamp used for illumination. Typical results varied by >15% across a series of repeated scans, with an overall decrease in

emission intensity as illumination time increased. For this reason, the spectra for quantum yield determinations were recorded at high scan speeds and the excitation intensity attenuated relative to typical data-collection conditions. These precautions proved adequate to obtain reliable quantum yields. Each quantum yield was determined from the average of three sequential measurements on the same sample, which did not differ by more than 1% in any of the solvents studied. In nearly all cases, two independent measurements of the quantum yields were made, and the results typically agreed to within ±7%. No degradation was observed in the samples used for kinetic measurements.

As discussed in section III.B, the quantum yields measured here are systematically lower than the majority of available literature values. We therefore took a number of steps to eliminate possible systematic errors from these measurements. First, given the photodegradation problem, which was not mentioned in earlier studies, we took pains to determine whether an impurity in our samples might be the cause of both the degradation and the low quantum yields. Repeated recrystallization of the DPB as well as sublimation did not change the extent of the photodegradation or the quantum yields observed. We also obtained DPB samples from an independent manufacturer, Lanchaster Synthesis (98%), as well as multiple samples having distinct lot numbers from Aldrich. After purification, all of these DPB samples yielded identical results. We also considered the purification of the solvents used here but found that they, too, had little effect on the results. For example, a sample made by using hexane distilled under dry argon and subjected to three freeze/pump/thaw cycles displayed identical behavior to undistilled samples run without the freeze/pump/thaw procedure. From these observations, we concluded that the photodegradation process is intrinsic to DPB and is little affected by dissolved oxygen. The low quantum yields we observed, therefore, did not seem to be related to this degradation. We also carefully checked our methods of quantum yield determination. In contrast to disagreements with reported values in the case of DPB, we found that measurements on other well-studied compounds, for example, perylene and coumarin 153, yielded agreement with literature values to within ±5%. As a final check, we also sent DPB samples to two independent laboratories where quantum yields in hexane and cyclohexane were measured. The values measured there were within uncertainties of the values measured in-house. All of these checks point to the reported values being accurate to ±10%.

Time-resolved experiments were conducted using the time-correlated single photon counting method. An argon ion laser (Coherent Innova 400, 11.5W CW) was used to pump a mode-locked Ti:sapphire oscillator (Coherent Mira 900F, 1.2W ML, <200 fs). The output was pulse selected (Coherent 9200, 0.4W) and tripled (U-Oplaz TP-1B) to produce >0.5 mW of excitation light at 295 nm. Emission was passed through an adjustable polarizer and appropriate excitation filter, and then the wavelength was selected with a single monochromator (ISA H-10) having a resolution of ±4.0 nm and detected with a microchannel plate PMT (Hammamatsu R3809U). Emission was collected near the spectral maximum (and away from solvent Raman contributions). Instrumental resolution was typically 25 ps, as measured by the fwhm of the response to a dilute scattering solution.

Kinetic parameters related to DPB rotation and isomerization were determined from emission transients by using iterative reconvolution fitting techniques. Decays measured at magic angle polarization and near to the peak of the emission spectrum were found to be single-exponential functions of time. (When the emission was observed on the red edge of the spectrum ($I/I_{max} < 1/2$) an additional 10−20 ps component could sometimes be detected. It seems reasonable to ascribe this fast component to vibrational or perhaps torsional relaxation.[33,34]) Uncertainties in the measured time constants are estimated to be ±5%. Radiative and nonradiative rates were determined from the observed time constants of these decays τ_{fl} and the emission quantum yields via the relations $k_{rad} = \Phi_{fl}/\tau_{fl}$ and $k_{nr} = \tau_{fl}^{-1} - k_{rad}$. Rotation times were determined from polarized emission transients in two ways. In the first method, decays measured at parallel, perpendicular, and magic-angle polarizations were simultaneously fit to extract both the anisotropy and population decay parameters. Because of instrumental drift, we sometimes observed time shifts among the three decays, which rendered this approach unsatisfactory. In these cases, a second method of analysis was used instead. This latter method involves first fitting the magic-angle decay to determine the population relaxation time (τ_1) and then using this information in a constrained fit of the parallel polarized decay.[9] For a single-exponential anisotropy decay with initial anisotropy r_0 this biexponential should have time constants of τ_1 and $\tau_2 = (\tau_1^{-1} + \tau_{rot}^{-1})^{-1}$ and relative amplitudes $a_2/a_1 = 2r_0$. In cases where drift was not a problem, the results obtained with this alternative method typically agreed with results from simultaneous fitting to ±5%. Both methods of fitting were initially applied without constraining the value of r_0. In solvents where rotation was slow relative to the instrumental time resolution, the values of r_0 were close to the value of 0.39 reported by Anderton and Kauffman[20] on the basis of steady-state measurements in frozen solution. In the final analyses we therefore constrained r_0 to this value to reduce the uncertainty in measurements of fast rotation times. Uncertainties in measured rotation times are estimated to be ±10%.

Refractive indexes of the perfluoroalkane solvents and solvent mixtures (20 ± 0.5 °C) were measured by using an Abbe refractometer modified to enable measurement of low-index liquids. Uncertainties are expected to be ±0.002.

III. Results and Discussion

III.A. Steady-State Spectra. Representative absorption and emission spectra of DPB in the gas phase[31] and in several liquid solvents are provided in Figure 1. Some characteristics of these spectra are also listed in Table 1. Absorption and emission spectra display approximate mirror symmetry in all cases. Spectral shapes are similar in the gas phase and in liquid solution, with the main difference being an overall frequency shift. In most solvents, the shift from the gas phase can be accurately correlated using dielectric continuum descriptions.[47] In particular, we find that the solution-phase frequencies, measured here as peak frequencies, are well represented by

$$\nu - \nu_{gas} = af(n_D^2) + b\{f(\epsilon) - f(n_D^2)\} \quad \text{with } f(x) \equiv \frac{x-1}{x+2} \quad (2)$$

Fits to this expression, using gas-phase frequencies from the work of Itoh and Kohler,[31] are shown in Figure 2. The constants a and b ($/10^3$ cm^{-1}) derived from such fits are:

	N	ν_{gas}[31]	a	b	±
absorption	33	32.53	−9.86	−0.36	0.05
emission	16	28.64	−8.74	−0.35	0.06

(N denotes the number of data points and ± is the standard error of the fit.) Included in these fits are data in the alkane

TABLE 1: Summary of Results at 20 °C

solvent	n_D[a]	η/cP[a]	V_m dm^3 mol^{-1}[a]	ν_{abs} /10^3 cm^{-1}[b]	ν_{em} /10^3 cm^{-1}[b]	Φ_{fl}[c]	τ_{fl} /ns[d]	k_{rad} /10^8 s^{-1}[e]	k_{nr} /10^8 s^{-1}[e]	τ_{rot} /ps[f]
n-pentane	1.357	0.22	115	30.63	26.94	0.23	0.49	4.7	15.6	14
n-hexane	1.375	0.31	131	30.57	26.87	0.28	0.53	5.3	13.5	26
n-heptane	1.388	0.41	147	30.49	26.84	0.34	0.59	5.9	11.2	30
n-octane	1.398	0.55	163	30.45	26.78	0.36	0.63	5.7	10.3	36
n-nonane	1.406	0.71	179	30.42	26.76	0.39	0.67	5.7	9.2	50
n-decane	1.412	0.91	195	30.37	26.73	0.42	0.70	6.1	8.2	58
n-dodecane	1.422	1.50	227	30.36	26.69	0.43	0.76	5.7	7.5	83
n-tetradecane	1.429	2.34	260	30.32	26.65	0.48	0.80	6.0	6.5	110
n-hexadecane	1.434	3.42	293	30.28	26.62	0.51	0.82	6.2	6.0	134
methylcyclohexane	1.423	0.70	129	30.39	26.69	0.33	0.59	5.6	11.3	52
cyclohexane	1.426	0.98	108	30.37	26.71	0.39	0.63	6.1	9.8	57
2-methylbutane	1.354	0.24	116	30.66	26.98	0.25	0.45	5.6	16.5	
perfluoro-*n*-pentane	1.240	0.50	177	31.53	27.60	0.039	0.19	2.1	51	28
perfluoro-*n*-hexane	1.252	0.71	200	31.48	27.66	0.038	0.20	1.9	48	39
perfluoro-*n*-heptane	1.262	1.02	223	31.41	27.58	0.031	0.22	1.4	45	57
perfluoro-*n*-octane	1.267	1.47	251	31.37	27.56	0.037	0.24	1.6	41	80
perfluoro-*n*-nonane	1.274	2.11	269	31.36	27.59	0.048	0.25	1.9	38	101
p.f.-methylcyclohexane	1.282	0.87	195	31.40	27.56	0.058	0.21	2.8	46	
perfluoro hexanes	1.254	0.70	201	31.48	27.65	0.043	0.20	2.2	48	
perfluorodecalin	1.314	5.14	236	31.23	27.47	0.040	0.16	2.6	62	
perfluorotributylamine	1.292	5.50	355	31.35	27.54	0.068	0.24	2.8	38	

[a] n_D, η, and V_m are the refractive index, viscosity, and molar volumes of the solvents, mostly from literature sources. Refractive indexes of the alkane solvents were obtained from refs 101 and 102; those in perfluoro solvents were measured in-house. Viscosities were from ref 102 in the case of the alkanes and from refs 2, 103, and 104 for the perfluoroalkanes. [b] ν_{abs} and ν_{em} are the peak frequencies of the absorption and emission spectra ($\pm$50 cm^{-1}). [c] Φ_{fl} is the emission quantum yield ($\pm$10%). [d] τ_{fl} is the emission decay time ($\pm$5%). [e] k_{rad} and k_{nr} are the radiative and nonradiative rate constants. [f] τ_{rot} is the rotation time ($\pm$10%) of DPB in these solvents.

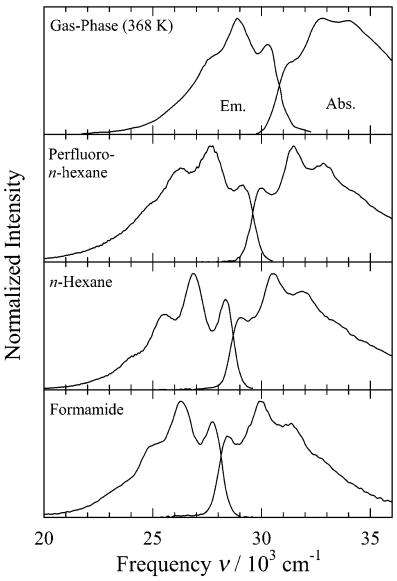

Figure 1. Representative absorption and emission spectra of DPB in the gas phase and solution. The gas-phase spectra are thermalized spectra at 368 K, recorded by Itoh and Kohler.[31] The remaining spectra were recorded at 293 K.

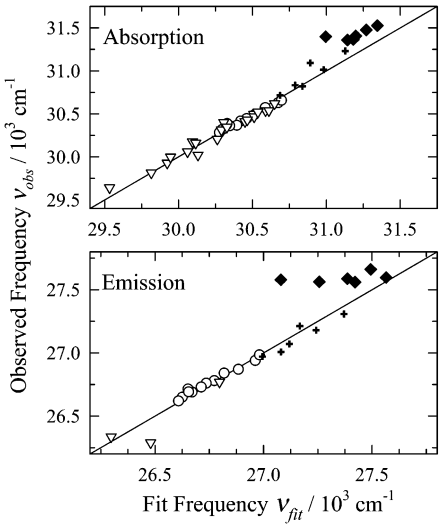

Figure 2. Absorption and emission (peak) frequencies of DPB in a variety of solvents, correlated according to eq 2. Open circles and filled diamonds, respectively, denote the alkane and perfluoroalkane solvents listed in Table 1. Crosses denote mixtures of perfluorohexanes + 2-methylbutane and perfluoromethylcyclohexane + hexane and triangles denote a variety of polar aprotic and protic solvents: carbon tetrachloride, acetonitrile, and formamide in emission and these solvents plus 1,1,2-trichlorotrifluoroethane, 1,1,1-trichloroethane, 1-chlorobutane, tetrachloroethylene, 1,2,4-trichlorobutane, di-isopropyl ether, diethyl ether, tetrahydrofuran, acetone, methyl acetate, ethyl actetate, dimethylformamide, dimethyl sulfoxide, propylene carbonate, methanol, and 1-propanol in absorption.[8] All data were recorded at 293 ± 2 K.

solvents listed in Table 1 (open circles in Figure 2), together with a range of polar aprotic and protic solvents (triangles). Excluded are the perfluoroalkane solvents (filled diamonds, Table 1) and the perfluoroalkane and alkane mixtures (crosses). It is clear from Figure 2 that the transition frequencies in perfluoroalkane solvents, especially in emission, are not accurately predicted by the same dielectric correlations that describe the shifts observed in the remaining solvents. Such nonconformity is not unique to the spectroscopy of DPB. It has been observed previously in the spectra of a number of aromatic hydrocarbons[5,6] and is suggested to reflect a different balance of attractive versus repulsive interactions in perfluoroalkanes compared to the balance of these interactions in other solvents.[6,48] As indicated by the relative magnitudes of *a* and *b* in eq 2, the spectral shifts of DPB are dominated by interactions with the electronic polarizability of the solvent (*a*). The permanent charge polarizability contribution (*b* term) is small, but inclusion of this term is required to achieve a good fit to these data.

An unusual feature of this solvent dependence is the fact that the peak of the absorption spectrum shifts considerably more

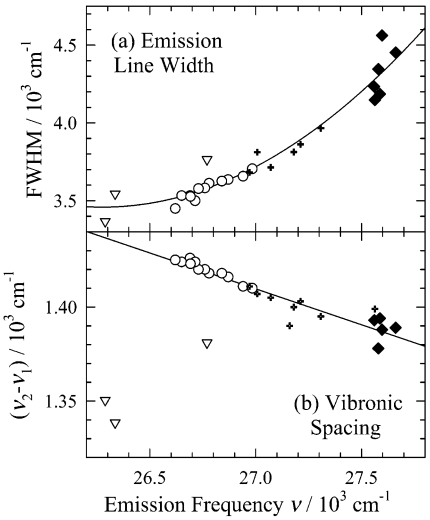

Figure 3. Solvent dependence of the width and vibronic spacing of the emission band of DPB plotted versus (peak) emission frequency (293 ± 2 K). The width is measured as the full width at half-maximum intensity and the vibronic spacing is the separation between the 1st and 2nd vibronic maxima. Symbols represent different solvent classes as described in Figure 2. The curve through the width data is a parabolic fit to all of the liquid-phase data. In the bottom panel the linear regression to all of the nonpolar liquid-phase data as well as the gas phase (not shown) is indicated.

with solvent than does the peak of the emission spectrum.[49] Closer inspection reveals the reason for this behavior is that the emission line shapes are not independent of solvent. (To a good approximation, the absorption line shapes are solvent independent.) As exemplified by the perfluoro-*n*-hexane data in Figure 1, the emission band is noticeably broader in perfluoroalkane solvents than in other solvents or the gas phase. But this excess breadth is not a peculiarity of perfluoroalkane solvents. Rather, the perfluoroalkanes represent one extreme of a systematic change in vibronic structure with emission frequency. As illustrated in Figure 3a, the width of the emission spectrum in liquid solvents increases continuously with emission frequency or decreasing solvent polarizability. It is not clear why this trend is not continued into the gas phase, where the width of the emission spectrum (at 368 K) is 3600 cm^{-1}, much narrower than indicated by the solution-phase correlation. Curiously, this broadening with increasing emission frequency is attended by a *decrease* in the spacing of the main vibronic features in the spectrum. The latter behavior is displayed in Figure 3b, where we plot the frequency difference between the two lowest-frequency peaks in emission. This trend *is* continued into the gas phase, where the observed spacing (1340 cm^{-1}) fits nicely on the linear correlation shown in Figure 3b. But polar solvents, symbolized by the open triangles in Figure 3b, do not appear to follow the same trend. The changes to the vibronic structure depicted here can also be monitored in terms of the relative heights of the first two vibronic peaks, which vary systematically with emission frequency or solvent polarizability. This intensity variation was previously noticed by Itoh who, like us, compared spectra in perfluoroalkane and alkane solvents.[32] It seems reasonable to ascribe these changes in the emission line shape to solvent-induced changes in the mixing of the nearly degenerate $2A_g$ and $1B_u$ states making up S_1. We will discuss this interpretation further in the next section after presenting results on the solvent dependence of radiative rates.

Before doing so, we note that the presence of ground-state *s-cis* isomers, detected in several previous studies,[50−52] might also be responsible for some of the changes in emission shape with solvent. The *s-cis* isomer emits to the red of the *s-trans* isomer and, if the *s-cis* fraction were to increase with decreasing solvent polarizability, solvent-dependent broadening of the sort observed would result. However, this possibility can be ruled out for several reasons. Sun and co-workers,[52] who performed detailed analyses of the emission of DPB in alkanes and toluene, showed that even above 90 °C the fraction of the steady-state emission contributed by this less-stable isomer is negligible unless emission is excited on the extreme red edge of the absorption band. In perfluoroalkane solvents, we observed no excitation wavelength dependence on the shape of the emission spectrum that would suggest the presence of more than one emitting species. Furthermore, the lifetime of *s-cis* isomers is 9 ns in cyclohexane.[51] Assuming comparable lifetimes in perfluoroalkane solvents, such a slowly decaying component would be noticeable in the time-resolved emission, but we find no such component in the data.

III.B. Emission Quantum Yields and Radiative Rates. More information about the solvent dependence of the state(s) responsible for the emission of DPB is contained in the behavior of the radiative rates. By radiative rate here, we simply mean the value obtained from the relation $k_{rad} = \Phi_{fl}/\tau_{fl}$, where Φ_{fl} and τ_{fl} refer to the overall yield and lifetime of the fluorescence, whatever its origins. Before discussing these data, we first digress to note that the radiative rates determined here differ from commonly accepted literature values. In Table 2 we compare our quantum yields and lifetimes and the resulting radiative rates to available literature data. The first entry in each column is the value measured in the present study. The quantum yields in *n*-hexane and cyclohexane in parentheses are measurements made on our samples by other laboratories. The majority of the comparable data from the literature is from the well-known early study by Velsko and Fleming.[10] In comparing our data to theirs, we find that the main point of disagreement is in the quantum yield values. Our quantum yields are systematically ~19% lower than those reported in the Velsko and Fleming paper. Although our lifetimes are also systematically ~7% larger than the values reported by Velsko and Fleming,[10] this latter difference is expected based on the temperature difference between the measurements: 20 °C here versus 24 °C in ref 10. The radiative rates calculated from our quantum yields and lifetimes are an average of 23% smaller than those reported by Velsko and Fleming. Radiative-rate data from other sources[53−55] are too scarce to be of help in understanding the origin of this discrepancy, but it must be admitted that other published quantum yield data appear to support the higher values of Velsko and Fleming rather than our values. This disagreement is troubling, and we still have no explanation for it, but as discussed in section II, we have gone to considerable lengths to verify the correctness of our results, and we believe they are to be preferred.

Figure 4 summarizes the radiative rate data we have collected in alkane solvents (open symbols), perfluoroalkanes (filled diamonds), and alkane and perfluoroalkane mixtures (crosses). Also shown (hexagon near the origin) is the radiative rate of isolated DPB determined by Amirav et al.[27] Although the latter value pertains to the jet-cooled molecule, the rate was found to be independent of excess energy over the entire range of 0−7500 cm^{-1}, which suggests that it can be compared to thermalized data. It is clear that the radiative rates, like the emission line shape features discussed previously, vary systematically with solvent polarity or polarizability in these nonpolar solvents. In Figure 4, we use the Clausius−Mossotti factor $f(n^2) = (n^2 - 1)/(n^2 + 2)$ to quantify the solvent effect rather than

TABLE 2: Comparison of Fluorescence Quantum Yields, Lifetimes, and Radiative Rates (20 °C) to Literature Values[l]

solvent	quantum yield Φ_{fl}	fluorescence lifetime τ_{fl}/ps	radiative rate $k_{rad}/10^8$ s^{-1}
n-pentane	0.23 ± 0.02 0.35 (24 °C)[a]	492 ± 15 450 (24 °C)[a], 440 (22 °C)[2]	4.7 ± 0.4 7.8[a]
n-hexane	0.28 ± 0.02 (0.31[c], 0.26[d]) 0.35 (24 °C)[a], 0.37 (?)[e], 0.37 (22 °C)[k]	533 ± 18 485 (24 °C)[a], 530 (?)[e], 480 (22 °C)[b], 511 (20 °C)[f], 469 (?)[g], 465 (?)[h]	5.3 ± 0.5 7.2[a], 7.0[e]
n-octane	0.36 ± 0.03 0.45 (24 °C)[a]	626 ± 18 580 (24 °C)[a], 565 (22 °C)[b]	5.7 ± 0.5 7.7[a]
n-decane	0.42 ± 0.04 0.51 (24 °C)[a]	700 ± 15 630 (24 °C)[a], 660 (22 °C)[b]	6.1 ± 0.6 8.1[a]
n-tetradecane	0.48 ± 0.04 0.56 (24 °C)[a]	796 ± 24 740 (24 °C)[a]	6.0 ± 0.5 7.6[a]
n-hexadecane	0.51 ± 0.04 0.59 (?)[d]	823 ± 25 910 (?)[d]	6.2 ± 0.6 6.5[e]
cyclohexane	0.39 ± 0.03 (0.38[c], 0.39[d]) 0.42 (24 °C)[a], 0.42 (22 °C)[i], 0.44 (23 °C)[j]	629 ± 19 570 (24 °C)[a], 600 (22 °C)[i]	6.1 ± 0.6 7.4[a]
methylcyclohexane	0.33 ± 0.03 0.39(22 °C)[k]	593 ± 18	5.6 ± 0.5

[a] Reference 10. [b] Reference 16. [c] Z. Gryczynski, private communication, 2002. [d] R. Moog, private communication, 2002. [e] Reference 53. [f] Reference 105. [g] Reference 33. [h] Reference 28. [i] Reference 106. [j] Reference 59. [k] Reference 52. [l] The first row in each case is the value obtained in the present study. Quantum yields in *n*-hexane and cyclohexane were also measured using our samples in other laboratories (footnotes c and d), and values obtained in this way are listed in parentheses immediately after our values. All other values were obtained from the references cited. When temperatures were explicitly provided in the references they are listed in parentheses. A question mark designates that only "room temperature" or no indication at all was provided.

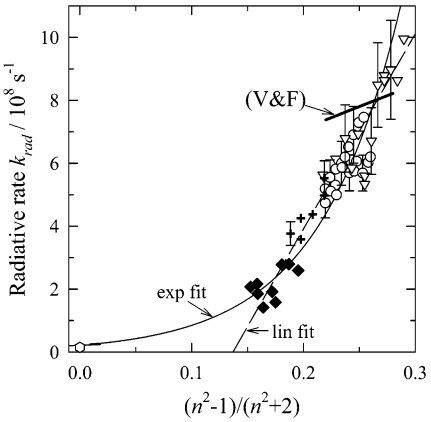

Figure 4. Radiative rate constants of DPB as a function of the electronic polarizability factor $(n^2 - 1)/(n^2 + 2)$. Open circles denote data in *n*-alkane solvents, open triangles are other alkanes, filled diamonds are perfluoro-*n*-alkanes, and crosses are alkane + perfluoroalkane mixtures. The representative error bars shown here reflect estimates of ±5% in total emission decay rates and ±10% or ±15% (low-temperature data) in the quantum yields. See the text for further details.

emission frequency as was done in Figure 3. A comparable correlation is obtained using observed emission frequencies; however, the present representation facilitates estimation of radiative rates in cases where spectral data are unavailable. For such purposes we have fit these data to both linear (ignoring the isolated molecule result) and exponential functions:

$$k_{rad}/10^8\,s^{-1} = -7.08 + 54.9f(n^2) \quad (N = 51; \pm 0.68) \qquad (3a)$$

$$k_{rad}/10^8\,s^{-1} = 0.214\,\exp\{13.8f(n^2)\} \quad (N = 50; \pm 19\%) \qquad (3b)$$

No particular model is implied by these fitting functions; however, the exponential fit might be rationalized in terms of some sort of state mixing that depends exponentially on an energy separation. The functional form suggested by the polyene model of Andrews and Hudson,[56] $k_{rad} \propto (1/\{a + bf(n^2)\})$, has a clearer theoretical justification, but provides a poor representation of the present data. Where measured values are not available, we use a combination of both eqs 3a and 3b to estimate radiative rates. Finally, we note that the present parametrizations indicate a much more pronounced solvent dependence than the original fit of k_{rad} provided by Velsko and Fleming, $k_{rad}/10^8\,s^{-1} = 4.3 + 14f(n^2)$. This latter result is shown by the line labeled "V&F" in Figure 4. Differences in values of k_{rad} estimated from eq 3 versus those estimated from the commonly accepted V&F parametrization can lead to significant differences in the nonradiative decay (isomerization) rates one derives from total emission decay data in cases where k_{rad} and k_{nr} are comparable. This condition mainly occurs in the longer *n*-alkane solvents and in some compressed alkane solutions, where previously reported isomerization rates may require revision.

We now consider what the above results imply about the character of the emissive state(s) of DPB. In the gas phase, it is clearly established that the origin of the dipole forbidden $2A_g$ state lies ~1000 cm^{-1} lower in energy than the origin of the strongly allowed $1B_u$ state.[26,29,31] In room-temperature solution, it is much more difficult to assign the origins of these broad transitions, but 2-photon absorption spectra suggest that the origins are nearly coincident in cyclohexane,[57] whereas in CCl_4 the $2A_g$ state appears to lie above the $1B_u$ state by more than 2000 cm^{-1}.[58] These observations are in keeping with the recent suggestion of Itoh[32] that the crossover point between the gaslike situation, wherein the $2A_g$ state is lowest in energy, to a situation where $1B_u$ is the lowest state, occurs for solvents slightly less polarizable than the alkanes. The data collected here are also consistent with such a description. In most solvents the emission is close to what would be expected for the $1B_u$ state. Thus, the vibronic structure is close to a mirror image of that found in absorption where $1B_u$ dominates. In cyclohexane, the radiative rate $(5.6 \pm 0.7) \times 10^8$ s^{-1} is close to the value 6.6×10^8 s^{-1} expected for the $1B_u$ state based on a Strickler−Berg analysis of the absorption spectrum.[59] Although the variations shown in Figures 3 and 4 are continuous with solvent polarizability, the ~3-fold decrease in k_{rad} and the substantial increase in the width of the emission between the alkane and perfluoroalkane solvents makes it reasonable to suppose that the switch to a gas-like ordering occurs between these two solvent classes.

TABLE 3: Summary of Temperature Dependent Rotation Times[a,f]

solvent	T range/K[b]	N[c]	A	$B/10^4$	$\pm$[d]	R^2[e]	A_η	B_η
n-hexane	228−324	11	−12.1	3.725	1.9	0.996	−4.10	859
n-heptane	265−324	5	−1.4	2.202	1.8	0.981	−4.13	952
n-octane	265−324	5	−1.3	2.027	1.7	0.991	−4.29	1080
n-nonane	265−310	4	1.4	1.976	1.6	0.996	−4.44	1201
methylcyclohexane	253−353	6	−8.4	2.340	5.5	0.986	−4.39	1198
perfluoro-*n*-hexane	278−323	4	−8.7	1.985	0.6	0.999	−4.75	1292
perfluoro-*n*-heptane	278−348	5	1.8	1.611	2.0	0.994	−5.22	1529
perfluoro-*n*-octane	278−348	5	−1.1	1.462	5.5	0.979	−5.33	1708
perfluoro-*n*-nonane	293−348	4	1.0	1.401	3.2	0.993	−5.87	1928

[a] Rotation data are parametrized in terms of fits to the equation: $(\tau/\text{ps}) = A + \text{B}(\eta/T)/(\text{cP/K})$ where η is the solvent viscosity and T the temperature. [b] T range denotes the range of temperatures over which data were collected. [c] N is the number of data points. [d] $\pm$ is the standard error of the fit. [e] R is the correlation coefficient. [f] For convenience, we also show parametrizations of the viscosities of these solvents accurate over the temperature ranges indicated. The fitting function used here is: $\ln(\eta/\text{cp}) = A_\eta + \text{B}_\eta(\text{K/T})$. Data for these parametrizations came from ref 102 in the case of the alkanes and refs 2, 103, and 104 in the case of the perfluoroalkanes.

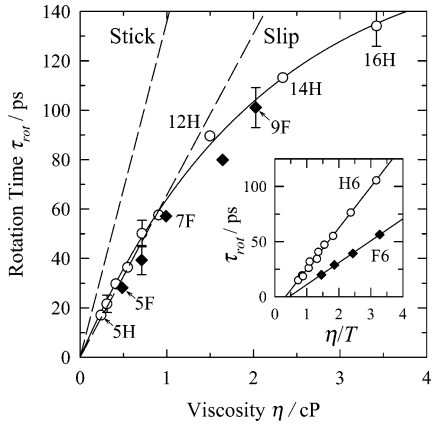

Figure 5. Rotation times of DPB in *n*-alkane (open circles) and perfluoro-*n*-alkane (filled diamonds) solvents. The main panel shows data at 20 °C plotted versus solvent viscosity (η). The inset shows temperature-dependent data plotted versus η/T (in units of 10^3 cP/K). Solvents are denoted by "12H" = *n*-$C_{12}H_{26}$, "9F" = *n*-C_9F_{20}, etc. The solid curve is a fit to the *n*-alkane data used as a visual guide, and the dashed lines are the hydrodynamic predictions described in the text.

It is not obvious what effect the near coincidence of these two states or a possible reversal in their ordering between the alkanes and perfluoroalkanes would have on the isomerization process in DPB. According to Gustaffson and co-workers,[33,34] the presence of vibrations characteristic of both electronic states in the resonance Raman spectra of DPB in hexane and THF is best interpreted by viewing S_1 to consist of a single, strongly mixed ($2A_g + 1B_u$) state rather than a thermal mixture of two distinct states. This description is at least consistent with our observations of the lack of wavelength dependence in the steady-state spectra or emission kinetics. For purposes of modeling the isomerization of DPB, we will adopt this viewpoint and assume, for want of more information, that reaction occurs on a single electronic surface of mixed $2A_g+1B_u$ character, whose composition varies systematically with solvent polarity.

III.C. Rotation Times and Solvent Friction. To examine the solvent dependence of the friction on DPB motion (which will be of importance for modeling the isomerization), we have measured rotation times in a variety of alkane and perfluoroalkane solvents at room temperature, as well as the temperature dependence of these times for the $n = 6-9$ series. Results are summarized in Tables 1 and 3 and in Figures 5 and 6. The dependence of DPB rotation times τ_{rot} on viscosity at 20 °C in the series of normal alkanes (open circles) and perfluoroalkanes (filled diamonds) is shown in Figure 5. As a starting point for understanding rotational friction, we employ the predictions of hydrodynamic theories, wherein the rotation time (or equivalently, the friction constant[60]) is proportional to the solvent's shear viscosity:

$$\tau_{\text{hyd},x} = \frac{V_u \eta}{k_B T} f_x \tag{4}$$

In this expression, V_u is the solute volume, η the solvent viscosity, k_BT the thermal energy, and f_x a shape factor for boundary condition x = slip or stick. Using an estimate of 205 Å^3 for the van der Waals volume of DPB and adopting an ellipsoidal model with semi-axis lengths of 8.2, 3.0, and 2.0 Å, the shape factors for slip and stick boundary conditions are 1.3 and 2.7, respectively.[61−63] These hydrodynamic predictions are shown as dashed lines in Figure 5. It is clear that neither prediction adequately describes all of the features of the experimental data. The slip predictions are close to the observed times for the shorter homologues (lower viscosities), but the proportionality to viscosity predicted by hydrodynamic models is not maintained in the longer *n*-alkane solvents ($n \geq 12$).[64] The sub-linear behavior (roughly $\tau_{rot} \propto \eta^{0.75}$) shown by the rotation times of DPB in the *n*-alkane series has been observed in other systems numerous times before.[25,65−68] There also appears to be a systematic difference between the rotation times of the *n*-alkanes and perfluoro-*n*-alkanes of the same viscosity. The difference is roughly within experimental uncertainties in the data recorded at 20 °C, but as shown on the inset to Figure 5, much larger differences can be observed at lower temperatures. Here one finds that for a given value of η/T, rotation times in a perfluoro-*n*-alkane solvent can be as much as a factor of 2 faster than in the corresponding *n*-alkane solvent.

Deviations from hydrodynamic predictions are to be expected given that the simple boundary conditions used in such calculations cannot accurately capture the frictional coupling between the solute and solvent, which should vary with a number of factors such as the relative size of the solute and solvent, the solvent density, and differences in solute−solvent interactions compared to solvent−solvent interactions. Nevertheless, these detailed local interactions ultimately dissipate the rotational or translational energy of a solute into the hydrodynamic modes of the larger surroundings.[69] For this reason, it is useful to empirically characterize rotational friction in terms of a coupling factor, C_{rot}, which measures degree of solute−solvent coupling relative to that predicted by stick hydrodynamics:[60]

$$\tau_{rot} \cong \frac{\eta V}{k_B T} f_{stick} C_{rot} + \tau_{free} \tag{5}$$

The fact that rotation times are limited by solute inertia as $\eta \rightarrow 0$ is approximately accounted for by inclusion of the free-rotor

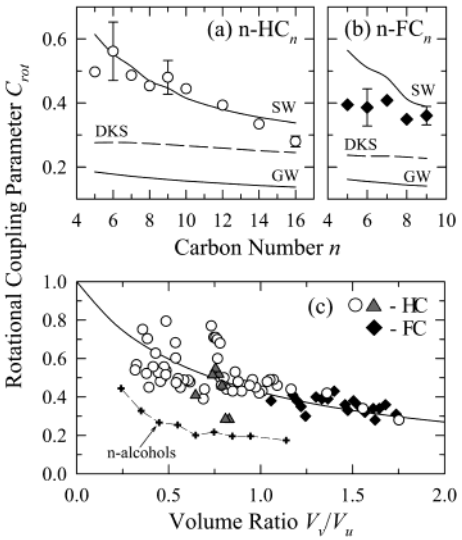

Figure 6. Observed rotational coupling factors (C_{rot}; eq 6) of DPB in a variety of solvents. Panels a and b are data in *n*-alkane (*n*-HC$_n$) and perfluoro-*n*-alkanes (*n*-FC$_n$) at 20 °C plotted versus carbon number *n*. The predictions of three models of C_{rot} described in the text are shown as solid or dashed curves on these panels. Panel c shows values of C_{rot} of DPB in *n*-alkane (open circles), other alkane (gray triangles), and perfluoro-*n*-alkane solvents (black diamonds) derived from rotation data at a variety of temperatures and densities. In addition to the temperature-dependent data measured here, we have included results derived from data of Schroeder et al.[15] in compressed liquid ethane, propane, and *n*-butane. Coupling factors are plotted against the solvent/solute volume ratio[78] as described in the text. Data in *n*-alcohol solvents (methanol − *n*-decanol) derived from the rotation times of Anderton and Kauffman[20] are also shown for comparison.

time $\tau_{free} \cong 0.83\sqrt{I_{eff}/k_BT}$.[70] For DPB, $I_{eff} = 1760$ amu Å^2, $\tau_{free} = 2.1$ ps at 20 °C. Operationally, we determine rotational coupling factors from observed times, τ_{obs}, by inverting eq 5 to read:

$$C_{rot} = \frac{\tau_{obs} - \tau_{free}}{\tau_{stick}} \quad \text{with} \quad \tau_{stick} \cong \frac{Vf_{stick}}{k_BT}\eta \qquad (6)$$

Figure 6 displays frictional coupling factors calculated in this way and compares them to several theoretical predictions. The top two panels of Figure 6 show C_{rot} data at 20 °C in *n*-alkane and perfluoro-*n*-alkane solvents. In the case of the normal alkanes, the rotational coupling factor decreases from approximately 0.6 to 0.3 as the length of the alkane chain varies between 5 and 16. Over the smaller size range available in the perfluoro-*n*-alkane solvents, C_{rot} is constant to within estimated uncertainties, $C_{rot} = 0.38 \pm 0.02$. The only theories amenable to easy comparison to these data are the early treatments of Wirtz and co-workers[71,72] and the more recent quasi-hydrodynamic theory of Dote, Kivelson, and Schwartz.[73] Predictions of these theories are shown as the connected lines in the top panels of Figure 6.

The Gierer−Wirtz (GW) model of rotational friction[72,73] considers how the friction on a rotating spherical molecule varies with the thickness of the (spherical) shells of solvent molecules that surround it. The result depends only on the relative sizes of solvent and solute molecules.[74] As illustrated in the top panels of Figure 6, the GW theory grossly underestimates the observed coupling factors, which is not surprising given that DPB is far from a spherical rotor. The second theory is the quasi-hydrodynamic free space model of Dote, Kivelson, and Schwartz[73] (DKS). This model, which is more appropriate for nonspherical solutes, is based on the idea that C_{rot} should depend on the volume required for solute rotation relative to the available free volume.[75] The DKS model has already been applied to the rotation of DPB in *n*-alcohol solvents by Anderton and Kauffman,[20] who found it to be fairly accurate. In the case of the *n*-alkanes and perfluro-*n*-alkanes, the model is less successful. Figure 6 shows that the values of C_{DKS} are smaller than the experimental values by about a factor of 2. In addition, the dependence of C_{DKS} on chain length in the *n*-alkane series is weaker than that of C_{obs}. The final set of calculations shown in the top panels of Figure 6 ("SW") are based on the semiempirical model of *translational* friction due to Spernol and Wirtz.[71,76] Sun and Salteil[77] showed that the relationship between bulk- and microviscosity predicted by this model provides good predictions for the *rotational* coupling factors of stilbene in *n*-alkanes. They further recommend it as a method for estimating the friction on isomerization reactions (and we will test its utility for this purpose in the next section). The Spernol−Wirtz calculations plotted in Figure 6 are for diffusion of a solute the size of toluene, which we use to model reactive friction. For this choice of solute C_{SW} is close to the observed rotational coupling factors in room-temperature *n*-alkanes. The quantitative agreement is poorer in the case of the perfluoro-*n*-alkanes, and in this case the dependence on chain length (solvent size) is exaggerated compared to that in the experiment.

Although none of the models just described provides an accurate description of rotational friction in all of the situations of interest here, they all suggest that the primary determinant of C_{rot} is the relative size of the solute and solvent. In Figure 6c, we therefore plot observed rotational coupling factors for a much wider range of solvents and conditions versus the solvent−solute size ratio V_v/V_u.[78] The data here comprise all of the solvents listed in Table 1 (20 °C), data collected at other temperatures (Table 2), as well as values derived from rotation times measured by Schroeder et al.[15] in compressed *n*-alkane liquids ($n = 2-4$). Despite the considerable scatter in these data (due partly to experimental errors), all of the data in the nonpolar alkane and perfluoroalkane solvents appear to be at least reasonably correlated using this single variable. The curve shown in this panel is a fit to the purely empirical relation:

$$C_{rot}^{-1} \cong 1 + 1.36(V_v/V_u) \qquad (7)$$

which represents the 83 data points shown here with a standard error of 0.10. (Similar dependence on V_v/V_u is found to fit analogous rotation data for a wide range of solute−solvent combinations.[65,79]) We will therefore use this correlation as a convenient way of estimating rotational friction constants when modeling reactive friction in the next section.

In the Introduction, we raised the question of whether aromatic solutes such as DPB are subject to unusually weak frictional forces in perfluoroalkane solvents. In the case of rotational friction the answer appears to be no. As shown in the inset to Figure 5 (and Table 3), under conditions where hydrodynamic theories would predict identical friction (i.e., equal η/T), rotation of DPB in perfluoroalkane solvents is considerably faster than rotation of the equivalent alkane of the same chain length. The difference is about a factor of 2 in the case of *n*-hexane and perfluoro-*n*-hexane but gets progressively smaller as chain length increases. However, as Figure 6c illustrates, this deviation from hydrodynamic predictions in the perfluoroalkanes appears to be linked to the solvent−solute size ratio in much the same manner as in the case of the alkanes. The difference between "equivalent" alkanes and perfluoroalkanes appears to reflect the difference in sizes (molar volumes) of the two species, rather than being indicative of particularly

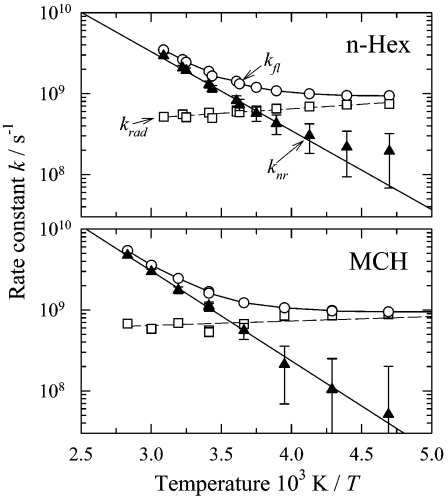

Figure 7. Arrhenius plots of the decay rates of DPB in *n*-hexane and methylcyclohexane (MCH). Total fluorescence decay constants (k_{fl}) are denoted by open circles, radiative rate constants (k_{rad}) by open squares, and nonradiative rate constants (k_{nr}) by filled triangles. The uncertainties shown for k_{nr} assume uncertainties of ±5% for k_{fl} and ±15% for quantum yields.

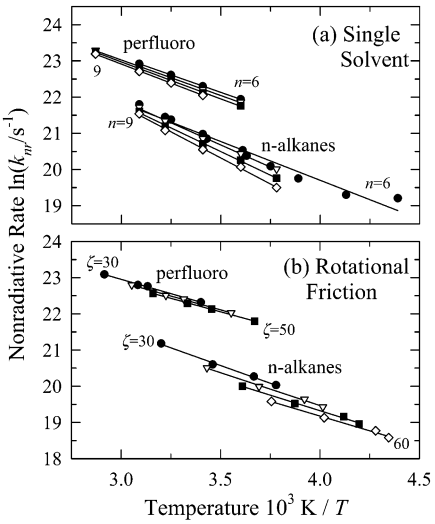

Figure 8. Arrhenius plots of the nonradiative decay rate constants of DPB in *n*-alkane and perfluoro-*n*-alkane solvents. Panel a shows a simple Arrhenius plot of data for the different solvents C_n, $n = 6-9$. Filled circles, open triangles, filled squares, and open diamonds label solvents $n = 6$, 7, 8, and 9, respectively. Panel b shows an "isofriction" representation of these data, as explained in the text. Here the different symbols label different values of rotational friction as filled circles = 30 ps^{-1}, open triangles = 40 ps^{-1}, filled squares = 50 ps^{-1}, and open diamonds = 60 ps^{-1}. The lines in both panels are linear regressions to the ln(k) versus $1/T$ data.

weak interactions in the perfluoroalkane case. A similar conclusion can be drawn in the case of translational friction based on measurements of the diffusion constants of biphenyl in *n*-alkanes and in perfluoro-*n*-hexane and perfluoro-*n*-nonane measured by Kowert and co-workers.[80,81]

It is interesting to contrast these results in nonpolar solvents to what is observed for rotation of DPB in alcohol solvents. Rotational coupling factors derived from the extensive data set recorded by Anderton and Kauffman[20] are also shown in Figure 6c. One finds that the rotational coupling constants of DPB in *n*-alcohol solvents exhibit a similar size dependence to those of the nonpolar solvents studied here, but overall magnitude of the coupling is reduced by a factor of 2−3. In contrast to the perfluoroalkane case, this difference does appear to reflect distinct frictional characteristics in *n*-alcohol solvents compared to alkanes. Ben-Amotz and co-workers[82] have previously noted similarly reduced friction on rotation of a number of other nonpolar solutes in alcohol solvents, a behavior they suggest might reflect preferential solvation of nonpolar solutes by the hydrophobic portions of these amphiphilic solvents. Whatever its origin, the fact that such differential coupling may exist among different solvent classes is relevant for the discussion of reactive friction in the next section.

III.D. Isomerization Rates. Information about the excited-state isomerization of DPB is obtained from observed emission decay rates after removal of the radiative decay component discussed in section III.B. The various contributions to the total emission decay are illustrated by the temperature-dependent data in *n*-hexane and methylcyclohexane shown in Figure 7. As illustrated here, radiative rates increase slightly with decreasing temperature, because of the increasing solvent density and refractive index. The nonradiative rates decrease much more rapidly. In methylcyclohexane, the emission quantum yield approaches unity to within experimental uncertainties (±15%) at low temperatures and the nonradiative rates exhibit an Arrhenius temperature dependence. In the case of *n*-hexane, the quantum yield is measured to be less than unity at the lowest temperature studied (210 K), which leads to a saturation in the nonradiative rate at a value of $\sim 2 \times 10^8$ s^{-1}. Similar behavior was also found by Velsko and Fleming,[10] who reported the nonradiative rate in *n*-hexane to depart from an Arrhenius dependence near 250 K. To account for this observation, Velsko and Fleming postulated a second, approximately temperature-independent nonradiative process in addition to the one dominant at high temperatures that is ascribed to isomerization. On the basis of this proposal, they and other workers[10,16,17] have sometimes chosen to subtract a temperature-independent value from nonradiative rate data to extract the isomerization rate. We do not follow this practice. Given the Arrhenius temperature dependence in methylcyclohexane, and the fact that the apparent leveling off in *n*-hexane is close to the (large) uncertainties in k_{nr}, we do not view this behavior as significant. Instead, we simply do not include the (highly uncertain) lowest temperature points in further analysis.[83] We assume that the measured nonradiative rates are dominated by a single process, excited-state isomerization, and analyze the behavior of $k_{nr} = k_{obs} - k_{rad}$ as a function of solvent and temperature. When quantum yields were not directly measured, the parametrization of $k_{rad}\{f(n^2)\}$ given by eq 3 is used for determining k_{nr}.

Figure 8a displays the temperature dependence of the nonradiative rates of DPB in the series *n*-alkane and perfluoro-*n*-alkane solvents having from 6 to 9 carbon atoms. The most obvious feature of these data is the fact that the nonradiative rates in perfluoro-*n*-alkanes are roughly 4-fold larger than those in the corresponding *n*-alkane solvents. (See also Table 1.) Over the ∼60 K temperature interval examined for most solvents, the data are well represented by an Arrhenius form,

$$k_{nr}(T) = A \exp(-E_{obs}/RT) \qquad (8)$$

Values of the constants A and E_{obs} are listed in Table 4. The activation energies (E_{obs}) obtained from such fits are in the range 20−24 kJ/mol in the *n*-alkanes studied, and they increase with increasing chain length. These results are comparable to results obtained by other workers. For example, Velsko and Fleming[10] reported 22−26 kJ/mol in several *n*-alkanes, and Allen et al.[53] measured the value 22 kJ/mol for DPB in cyclohexane over the range 288−338 K. Activation energies in the perfluoro-*n*-

TABLE 4: Summary of Fits to Nonradiative Rate Data

	simple Arrhenius[a]					isoviscosity[c]			isofriction[c]		
solvent	T range/K[b]	N[b]	% error[b]	A/ps^{-1}	E_{obs}/kJ mol^{-1}	η/cP	A/ps^{-1}	E_a/kJ mol^{-1}	ζ_{rot}/ps^{-1}	A/ps^{-1}	E_a/kJ mol^{-1}
						n-Alkanes					
n-hexane	227−324	11	4.0	4.01	19.6	0.3	2.56	18.5	20	1.95	18.0
n-heptane	264−323	5	4.0	5.02	20.4	0.4	1.37	17.1	30	0.81	16.3
n-octane	264−323	5	3.5	7.46	21.7	0.5	0.89	16.3	40	0.40	15.1
n-nonane	264−323	5	4.5	16.2	24.0	0.6	0.62	15.7	50	0.24	14.3
methylcyclohexane	233−353	9	20.	54.5	26.8	0.7	0.45	15.3	60	0.14	13.6
						Perfluoro-*n*-alkanes					
perfluoro-*n*-hexane	278−323	4	0.3	3.42	16.0	0.8	1.22	13.5	20	1.44	13.7
perfluoro-*n*-heptane	278−348	5	1.2	3.59	16.3	1.0	1.20	13.6	30	1.05	13.1
perfluoro-*n*-octane	278−348	5	1.7	4.36	17.0	1.2	1.10	13.5	40	0.83	12.7
perfluoro-*n*-nonane	293−348	4	1.0	4.91	17.5	1.4	1.03	13.4	50	0.71	12.4
						1.6	1.02	13.5	60	0.62	12.2

[a] Columns labeled "simple Arrhenius" refer to direct Arrhenius fits of observed nonradiative rate data. [b] T range, N, and % error here are the temperature range over which data were fit, the number of data points, and the standard error of the linear fit to ln k_{rad} versus T^{-1}. [c] Isoviscosity and isofriction are results of fits of interpolated nonradiative rate data at constant viscosity (η) and constant rotational friction (ζ_{rot}) as described in the text. In all cases, the fits were linear regressions to data in the format ln $k_{rad} = a + \epsilon/T$, and then the fitted values were reinterpreted as: $E_a = -R\epsilon$ and $A = \exp(a)$.

alkanes are roughly 25% smaller than in the *n*-alkanes and are less variable with chain length.

The energies derived in this manner indicate that the nonradiative process being observed involves a significant ($>5k_BT$) and possibly solvent-dependent activation barrier. If large amplitude motions are involved in the process, as would be expected for isomerization, these energies will contain contributions from changes to the friction on the reaction with temperature. Assuming that solvent friction "ζ" enters the problem in the manner

$$k_{nr}(\zeta,T) = A(\zeta)\exp(-E_a/RT) \tag{9}$$

one can attempt to extract the intrinsic barrier height E_a, i.e., the activation energy remaining when the frictional activation is removed, using an "isoviscosity" or "isofriction" analysis.[10] The reactive friction is not known accurately, but it can be estimated to within a constant of proportionality in one of two ways. The simplest approach is to assume that the friction is proportional to solvent shear viscosity η. In this case, constant friction is equivalent to constant viscosity, and Arrhenius fits of data for fixed η and variable T determine E_a. Alternatively, one can adopt what has come to be known as the "Hubbard" approximation[19,24,25] and assume that the relevant friction is proportional to the friction on solute rotation.[60,68,77] We approximate the latter by:

$$\zeta_{rot} \cong \frac{6k_BT}{I_{eff}}(\tau_{rot} - \tau_{free}) \tag{10}$$

where τ_{rot} is the observed (2nd rank) rotation time. Inserting the values of I_{eff} and τ_{free} described in the previous section, this expression can be specialized to:

$$\zeta_{rot}/\text{ps}^{-1} \cong 0.83\left(\frac{T}{293\text{ K}}\right)\left\{\tau_{rot}/\text{ps} - 2.1\sqrt{\frac{293\text{ K}}{T}}\right\} = 112C_{rot}(\eta/\text{cP}) \tag{11}$$

The second of these equations shows that the difference between isoviscosity and iso(rotational)friction representations is a constant times the rotational coupling factor defined by eq 6.

Figure 8b shows Arrhenius plots of data at constant rotational friction. The results at constant viscosity look similar and are not shown. As can be seen from the Arrhenius parameters listed in Table 4, both representations significantly reduce the apparent activation energies from those obtained with eq 8: by 5−6 kJ/mol in the case of the *n*-alkanes and by 3−4 kJ/mol in the perfluoroalkanes. (For comparison, the viscosity activation energies average 8.5 kJ/mol in the *n*-alkanes and 13.5 kJ/mol in the perfluoro-*n*-alkanes over this range of chain-lengths.[84]) The spread in the "intrinsic" activation energies E_a across the data sets is comparable to the spread in the original values of E_{obs}. In this sense, both of these methods for removing frictional contributions to the activation energy appear to overestimate its contribution in the *n*-alkanes. However, it could also be that frictional effects aside, the intrinsic barrier to reaction is not constant within the *n*-alkane series of solvents. The fact that activation energies found in alcohol and other polar solvents[11,17,19,22] are much smaller than the values in nonpolar solvents, together with the evidence for the changing character of the emitting state with refractive index presented in sections III.A and III.B, makes such a suggestion seem reasonable.

To proceed further, it is necessary to adopt a more definite model for the frictional dependence of the nonradiative decay. For this purpose we assume that the reaction can be described by the "spatial diffusion" regime of Kramers' barrier crossing theory.[85−89] In this case the nonradiative rate constant can be written

$$k_{nr} = \kappa(\zeta)\cdot k_{TST} = \kappa\cdot\frac{\omega_R}{2\pi}\exp(-E_a/k_BT) \tag{12}$$

where

$$\kappa = (x^2+1)^{1/2} - x \quad \text{with} \quad x = \frac{\zeta}{2\omega_b} \tag{13}$$

These expressions refer to an irreversible reaction over an (intrinsic) barrier of height E_a beginning from thermal equilibrium in a reactant well having frequency ω_R. The effect of solvent friction is contained in the transmission coefficient κ, which modifies the transition-state theory rate constant k_{TST} to an extent that depends only on the ratio of the friction on reaction ζ and the "frequency" ω_b of the reactive barrier.

Although this model is relatively simple, few of the parameters of the reactive potential or their solvent dependence are known independently of kinetic data. A variety of choices are therefore possible when fitting experimental data to the model, which renders the inferences drawn from such fits nonunique. After exploring a number of approaches, we settled on the

TABLE 5: Results of Kramers' Model Fits[a]

fit	species fit	ν	χ^2_ν	E_a^0/kJ mol^{-1}	a_E/kJ mol^{-1}	α *n*-alk	α *c,b*-alk	α perfl	α OH
1	*n*-alkanes	129	2.5	10.9	(0)	1.73	–	–	–
2	*n*-alkanes	128	1.2	7.43	37.4	0.173	–	–	–
3	*n*-alkanes (η)	128	1.6	7.13	40.16	0.056	–	–	–
4	*n*-alkanes (SW)	128	1.1	7.37	37.47	0.158	–	–	–
5	perfl-*n*-alkanes	17	0.63	11.7	0.00	–	–	0.086	–
6	perfl-*n*-alkanes	16	0.21	6.61	41.28	–	–	0.017	–
7	*c,b*-alkanes	11	1.1	14.4	(0)	–	0.184	–	–
8	*c,b*-alkanes	12	0.61	(7.43)	(37.4)	–	0.043	–	–
9	*n*-alcohols	75	1.5	(11.75)	−8.23	–	–	–	0.442
10	all solvents	236	2.5	11.9	−7.71	2.01	1.47	0.196	0.390

[a] ν is the number of degrees of freedom (no. of data points − no. of fitted parameters), χ^2_ν reflects the quality of the fit,[92,93] and the remaining values are parameters of the model described by eqs 12−16. Values in parentheses are held constant in the fitting. (In all cases the value of $\omega_R^0$is fixed at 5 ps^{-1} and is therefore not listed.)

following parametrization as the best compromise between maintaining sufficient flexibility to fit the observed data while at the same time constraining enough of the parameters to avoid unrealistic descriptions. First, we assume that the activation energy, the parameter having the largest impact on the rates, can be described by a linear function[90] of solvent polarity or polarizability:

$$E_a(\epsilon) = E_a^0 + a_E f(\epsilon) \qquad f(x) = (x-1)/(x+2) \quad (14)$$

(The static dielectric constant ϵ appears here for later convenience; for the nonpolar alkane and perfluoroalkane solvents we assume $\epsilon = n^2$.) To minimize the number of fitting parameters, we require that the frequencies ω_R and ω_b vary as they would if the effect of solvent is to merely alter the energy scale of the potential:

$$\frac{\omega_R(\epsilon)}{\omega_R^0} = \frac{\omega_b(\epsilon)}{\omega_b^0} = \left(\frac{E_a(\epsilon)}{E_a^0}\right)^{1/2} \quad (15)$$

We further assume that the reactive friction ζ is proportional to the rotational friction as specified by eq 10. To analyze cases where no rotation data are available, we further assume that $\zeta_{rot} \propto C_{obs}\eta$, as in the 2nd line of eq 11. Finally, because ζ and ω_b enter the theory only as the ratio ζ/ω_b, we use for the solvent dependence of the friction variable x:

$$x \equiv \frac{\zeta}{2\omega_b} = \alpha\frac{\zeta_{rot}}{2\omega_R(\epsilon)} \qquad \text{with } \alpha = \frac{\zeta}{\zeta_{rot}}\frac{\omega_R^0}{\omega_b^0} \quad (16)$$

There are thus four adjustable parameters in this model: E_a^0, a_1, ω_R^0, and α. Of these parameters, E_a^0 and ω_R^0 are constrained by the expectation that they should lie close to the gas-phase values $E_a^0 = 11.5-12$ kJ mol^{-1} and $\omega_R^0 = 4.3-5.5$ ps^{-1} deduced from RRKM analysis of the isolated-molecule rate.[13,14,18] Given the strong correlation between the values of E_a^0 and ω_R^0, we adopted a fixed value of $\omega_R^0 = 5.0$ ps^{-1}, thereby reducing the number of adjustable parameters actually used in fitting to three.

To provide the most meaningful fits possible, in addition to our own data, we have reanalyzed the large amount of data on DPB isomerization in *n*-alkane solvents already available in the literature.[10,12,14,16] The collected data include liquid alkanes $n = 5-16$ under ambient conditions, compressed liquid *n*-alkanes from $n = 2-11$ near to room temperature[91] as well as the temperature-dependent data displayed in Figure 8. In all cases, we have applied the procedures described above for determining k_{nr} from k_{obs} by using eq 3 to represent k_{rad}. Values of the rotational friction are estimated from solvent viscosity using eq 11 and the empirical correlation eq 7. A summary of all of the compiled data are provided as Supporting Information Table S-1. These data were fit using a weighted least-squares algorithm, assuming uncertainties in the values of k_{obs} to be ±5% and in k_{rad} to be ±12%. Results obtained in this manner are summarized in Table 5 and illustrated in Figures 9 and 10.

The first thing evident upon attempting such a fit was that a satisfactory representation of the alkane and perfluoroalkane data is not possible using a single set of model parameters. We therefore first fit each solvent type independently, obtaining the results listed as fits 1−8 in Table 5. The largest number of data are available in *n*-alkane solvents (131 points), and we consider this data set first. Fit 1 to the *n*-alkane data uses a solvent-independent activation energy (E_a^0 and α varied, $a_E = 0$). Such a fit does not represent the *n*-alkane data to within the estimated uncertainties, as indicated by value of the χ^2_ν statistic,[92,93] being substantially greater than unity. Allowing for a linear dependence of E_a^0 on solvent polarizability (fit 2) does enable the model to describe the *n*-alkane data approximately to within its uncertainties. We will therefore initially regard fit 2 as the best representation of the data.

Figure 9 (open circles) illustrates the nature of fit 2. Figure 9a shows the observed versus calculated rates, and its inset shows the solvent dependence of E_a^0 and ω_R, which best fit the data. Figure 9b compares the transmission coefficients derived from the observed rates (points)

$$\kappa_{obs} = \frac{2\pi}{\omega_R(\epsilon)} e^{+E_a(\epsilon)/k_B T} k_{nr}^{obs} \quad (17)$$

to the model dependence of κ on ζ_{rot}/ω_R (curves). Note that the error bars increase substantially for small values of k_{nr} (high friction) because of the uncertainties introduced by subtracting the radiative component in the observed rates. Because of these large uncertainties, allowing a small constant component in the nonradiative rate to account for the possibility of an additional decay channel as mentioned at the start of this section, does little to improve (or alter) the fit. Except for the region of lowest friction ($\zeta_{rot}/2\omega_R < 1$), where the observed transmission coefficients in compressed ethane and propane[12,14] are more scattered than the estimated uncertainties, the fit to the *n*-alkane data is excellent. In this representation of the data, the Smoluchowski limit of Kramers' model, wherein $k_{nr} \propto \zeta^{-1}$, is not attained by most *n*-alkane solvents near room temperature. The value of $\alpha \approx 0.2$ (eq 16) indicated by the fit can be plausibly explained by assuming either that the reactive friction is considerably smaller than the rotational friction or that the barrier frequency is significantly larger than the well frequency. The

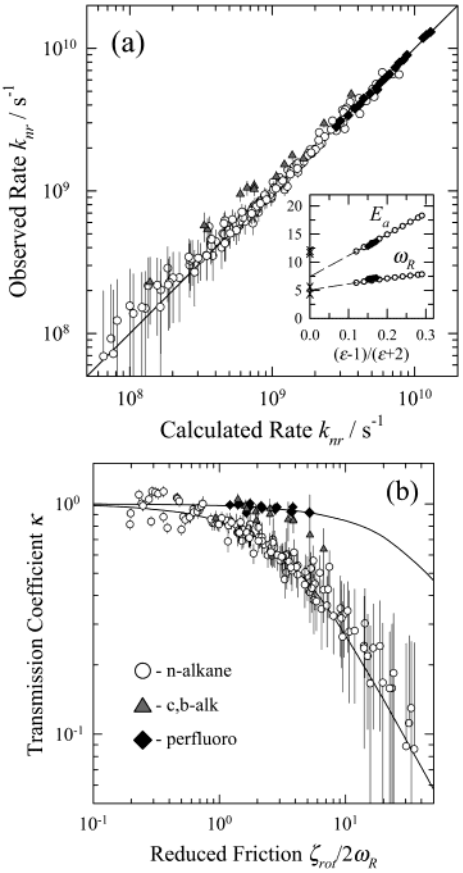

Figure 9. Results of fitting *n*-alkane (open circles) and perfluoro-*n*-alkane data (filled diamonds) separately to the Kramers' model described by eqs 12−16. Also shown but not included in the fitting are results for cyclic and branched alkanes (gray triangles). Panel a compares observed and calculated nonradiative rate constants k_{nr}, and panel b compares observed (points) and calculated (smooth curves) transmission coefficient, κ. The inset to panel a shows the solvent polarizability dependence of E_a and ω_R derived from these fits, with points indicating the range of values encompassed by each type of solvent. The points marked "X" at zero polarizability are the high-pressure limiting values from refs 14 and 18. *n*-Alkane data are from the present work and refs 10, 12, 14, and 16. Error bars assume uncertainties of ±5% in k_{obs} and ±12% in k_{rad}.

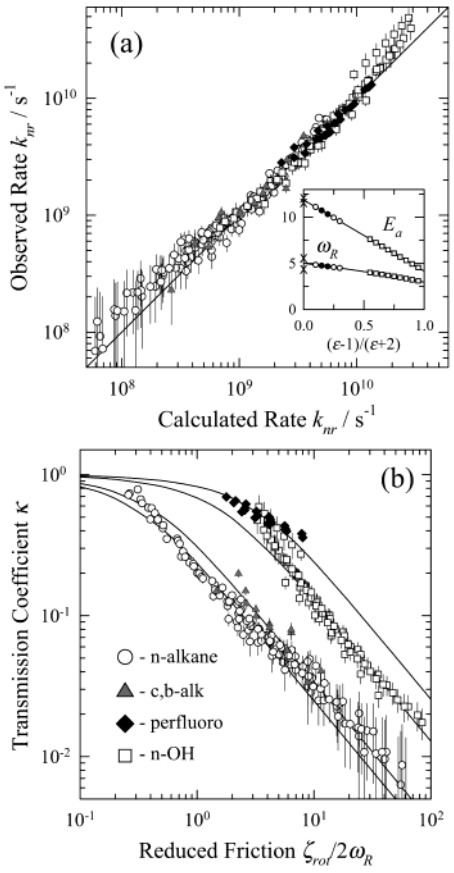

Figure 10. Results of "globally" fitting *n*-alkane (open circles), perfluoro-*n*-alkane (filled diamonds), and *n*-alcohol (open squares) data to the Kramers' model described by eqs 12−16 (see text). *n*-Alcohol data are from ref 19. Remaining details are the same as in Figure 9.

fit also predicts the activation energy (Figure 9a) to vary substantially (12−18 kJ/mol), with polarizability among the various *n*-alkane solvents and solvent conditions examined. This dependence is probably unrealistic, as will be discussed shortly.

Before doing so, it is important to note that the method employed for estimating solvent friction has only a modest impact on what one deduces about the reactive potential. This fact is illustrated by fits 3 and 4, which employ alternative friction representations for fitting the *n*-alkane data. Fit 4 assumes that the reactive friction is simply proportional to solvent viscosity (i.e., $C_{rot} = 1$). This approach degrades the quality of the fit noticeably, but the specification of the reactive potential in terms of $E_a(\epsilon)$ is largely unchanged. Use of the Spernol−Wirtz (translational) coupling factor[71] to model the reactive friction (fit 4) leads to fits of comparable quality to the use of the empirical rotational coupling factors via eqs 7 and 11. In fact, adopting the representation $\zeta \propto C_{SW}\eta$ leads to fits that are visually indistinguishable from those shown in Figure 9. In this case $E_a(\epsilon)$ is also nearly identical to that obtained from fit 2.

It is also interesting to compare the results of fitting the *n*-alkane and perfluoro-*n*-alkane data. As already mentioned, attempts to simultaneously fit data from both solvent types yields poor results ($\chi^2_\nu \approx 4$). Fits to the perfluoroalkane data alone are listed as fits 5 and 6 in Table 5. These independent fits to the perfluoroalkane data provide values of $E_a(\epsilon)$ (and thus $\omega_R(\epsilon)$) that nearly are indistinguishable from those obtained by fitting *n*-alkane data, as shown by the filled diamonds in the inset to Figure 9a. It is only the parameter α that must be appreciably changed from the *n*-alkane parametrization (reduced 10-fold) to fit the perfluoroalkane data. As illustrated by Figure 9b, the small value of α places the reaction close to the transition-state limit ($\kappa = 1$) in all of the perfluoro-*n*-alkane solvents. We note that a similar but more modest change in α is also required to achieve good agreement with data in cyclic and branched alkanes (c,b-alk in Figure 9b; fits 7 and 8).

Although the fits just described do reproduce a large number of data to within expected uncertainties, two features seem unrealistic. First, the activation energies deduced by fitting *n*-alkane data extrapolate a gas-phase value only ∼2/3 of the value expected from analysis of isolated-molecule data[13,14,18] (marked "X" on the inset to Figure 9a). More importantly, several studies have indicated that in polar solvents such as alcohols, the activation energy for DPB isomerization is smaller than in the alkanes,[11,17,19,22] just the opposite of what one would predict from fit 2. A final shortcoming is that the values of α required to fit the cyclic and branched alkanes, and especially the perfluoro-*n*-alkanes, seem unrealistically small (0.02 in fit 6).

A more satisfactory, albeit less accurate, representation of the data can be achieved by requiring that $E_a(\epsilon)$ behave sensibly in both the gas-phase limit and for values of ϵ characteristic of

polar solvents. To enforce the correct high-polarity behavior, we expanded the range of solvents examined to include the normal alcohols. For this purpose, we employ the data on isomerization rates and rotation times of DPB in the *n*-alcohol series methanol−decanol (263−343 K) measured by Anderton and Kauffman.[19,20] Anderton and Kauffman collected both types of data to perform an "isodielectric Kramers−Hubbard" analysis of the DPB reaction in alcohols quite similar in spirit to the fits attempted here. We have reanalyzed their data[94] and extracted smoothed values of k_{nr} as a function of ϵ and ζ_{rot},[95] using the methods described above for nonpolar solvents. (The availability of a complete set of $\tau_{rot}(T)$ makes it possible to determine ζ_{rot} directly for these data, i.e., without the need for an intermediate parametrization of C_{rot}.) After incorporating these alcohol results, we refit all of the available data simultaneously, assuming a dependence of the reactive potential on solvent polarity, $E_a(\epsilon)$, but allowing the factor α relating rotational and reactive friction to vary among the different solvent classes.

The result of such a global fit to both nonpolar and polar solvent data is listed as fit 10 in Table 5 and displayed in Figure 10. As indicated by the value of $\chi_\nu^2 > 2$, this global model does not fit all of the data to within estimated uncertainties. Figure 10 shows that both the *n*-alkane and *n*-alcohol data depart from the fit in a systematic manner at lower values of the friction. In both cases, the observed rates are faster than predicted. In the case of the alcohols, by far the largest discrepancy is in methanol (topmost row of points), where the calculated rates are ∼40% smaller than observed.[96] In the case of the *n*-alkanes we find that the rates in ethane[12,14] ($\zeta_{rot}/2\omega_R < 0.5$) average ∼15% higher than the predictions. The *n*-alkane data also appears to deviate systematically from the fit at high friction or low rate, but here the estimated uncertainties are typically larger than the deviations. Despite these imperfections, Figure 10 clearly demonstrates that this remarkably simple model of the solvent dependence reasonably correlates the nonradiative rates of DPB in quite a wide range of liquid solvents.

Before claiming undue generality, we must mention that two sets of data in supercritical solvents have been omitted from consideration. The first omission involves data in CO_2. Two groups[9,21] have measured the density dependence of rotation times and emission decay rates of DPB in supercritical CO_2 near to room temperature. Both groups reported rates of $\sim 1.5 \times 10^{10}$ s^{-1}, independent of solvent density over the range $0.5-2\rho_c$, were ρ_c is the critical density. Assuming that this density independence implies the transition state ($\kappa = 1$) limit, the above model (fit 10) would predict nonradiative rates that are ∼80% smaller than those observed. A reasonable explanation for this discrepancy is that the polarity of the quadrupolar solvent CO_2 is inadequately reflected in its dielectric constant.[97,98] Over the experimental data range the maximum value of ϵ is only ∼1.5; however, studies of solvatochromism indicate that CO_2 has an effective polarity comparable to dipolar solvents having dielectric constants in the range of 3−5.[98] If one uses such values of ϵ within the present model, E_a is reduced by the 1−2 kJ/mol needed to bring the CO_2 rates into agreement with the remaining solvents. Thus, these supercritical CO_2 data do not really conflict with the model. A more puzzling case is provided by the measurements of k_{nr} in supercritical ethane and propane at elevated temperatures (∼400 K) by Gehrke et al.[14] Especially in the case of propane, the measured rates are systematically higher than would be expected from the above model, in some cases by as much as a factor of 2. We do not have a good explanation for this deviation. Most data employed in fitting the present model were recorded in the ∼50 K temperature range between 265 and 323 K. At the significantly higher temperatures of their experiments, Gehrke et al. noted that the change in k_{nr} with temperature is much larger than anticipated. These authors suggested that changes to the barrier shape, as a result of activation of coordinates orthogonal to the reaction coordinate, might be the source of this enhanced temperature dependence. It could also be that additional nonradiative channels play a role at elevated temperatures. More experimental study will be required to understand these observations.

TABLE 6: Comparison of Kramers' Model Parameters

solvent	$f(\epsilon)$	E_a/kJ mol^{-1}[a]	ω_R/ps^{-1}	notes and references
gas	0	11.5	4.3	13
	0	12.0	5.5	18
perfluoro-*n*-alkanes	0.15 → 0.17	10.7 → 10.5	4.7	fit 10
		11.7	5	fit 5
		10.9 → 9.6	4.8 → 4.5	fit 10
n-alkanes	0.13 → 0.29	11.9 → 18.2	6.3 → 7.8	fit 2
		20 ± 2	124	12
		(13.8)*[b]	(12.7)*	24
		7.3 → 4.7	3.9 → 3.1	fit 10
		8.4 → 4.7	3.8 → 2.6	fit 9
n-alcohols	0.75 → 0.86	12.5 → 9	76 → 25	19
		>0.5	−	17
		2.9 ± 1.2	−	11

[a] The notation $E_a = 10.9 \rightarrow 9.6$ indicates the range of values of E_a corresponding to the range of $f(\epsilon)$ indicated. [b] Asterisks indicate data on the DPB analogue "stiff-6 DPB".

These subtleties aside, the one-dimensional Kramers' model, coupled to the simple dielectric parametrization of the reactive surface proposed here, does capture the essential features of the solvent dependence of the DPB reaction. We therefore finally consider the meaning of the model parameters derived from the present fits. Table 6 summarizes how the potential characteristics E_a and ω_R are predicted to vary among the different solvent types and makes some comparison to previous Kramers' theory analyses. The first two rows in Table 6 list values of ω_R and E_a appropriate to the high-pressure gas-phase limit as determined from RRKM analyses of isolated-molecule data[26,27] by Troe and co-workers.[13,14] Although it is not within the capabilities of electronic structure methods to predict E_a, a value of 29 cm^{-1} (∼5 ps^{-1}) was recently calculated for the reactive frequency ω_R in the $1B_u$ state,[18] which supports the validity of these gas-phase estimates. One would not expect ω_R to be greatly modified in solution, and the present model is consistent with this expectation. By virtue of the constraint placed on ω_R^0 and the fact that its solvent dependence is linked to that of E_a, ω_R is predicted to vary from 5 ps^{-1} at $\epsilon = 1$ to 3 ps^{-1} at $\epsilon = \infty$. We note that in earlier analyses, this parameter was allowed to adopt much larger, probably unrealistic, values (Table 6).

Fit 10 implies an activation energy which decreases from the gas-phase value of ∼12 kJ/mol down to ∼5 kJ/mol in the most polar alcohol solvents. This variation is larger than what was deduced from an analysis of the *n*-alcohol data by Anderton and Kauffman[19] but is somewhat smaller than that found by other authors.[11,17] In the present model, the dependence on solvent dielectric constant is given by:

$$E_a(\epsilon) = E_a^0 + a_E\left(\frac{\epsilon - 1}{\epsilon + 2}\right) \tag{18}$$

Such a dependence can be interpreted in terms of the dielectric continuum expression for the solvation free energy of polarizable dipolar solute:[99]

$$G \cong -\frac{\mu^2}{a^3}\left(\frac{\epsilon - 1}{\epsilon + 2}\right) \tag{19}$$

where μ is its dipole moment, and a, its radius. Assuming a nonpolar reactant state and estimating that $a \cong 3.7$ Å, based on the van der Waals volume of DPB, the magnitude of the fit parameter a_E implies a value of $\mu \approx 3$ D for the transition state of the reaction. Although this estimate is admittedly crude, it indicates a moderate polarity for the transition state in solution, consistent with its possessing significant zwitterionic character. Comparable but slightly larger variations in E_a are also indicated for the trans-stilbene reaction.[37]

The final and least certain aspect of this modeling concerns the need for distinct values of the frictional parameter α to adequately fit rates in the different solvent classes. As shown in eq 20, α is actually a product of two ratios: the ratio of gas-phase frequencies ω_R^0/ω_b^0, which is by construction solvent independent, times the friction ratio ζ/ζ_{rot}. Virtually nothing is known about the barrier frequency ω_b^0; however, it is unlikely to be greatly different from ω_R^0. If we make the simplest assumption possible, $\omega_R^0/\omega_b^0 \approx 1$, the values of α, which vary between 0.2 and 2, would directly reflect the relative friction on reaction compared to rotation. Are such values reasonable? Recent computer simulations of DPB in supercritical CO_2 suggest that they are at least of the proper magnitude. Patel and Maroncelli[8] simulated friction constants associated with rotation about all three of the inertial axes of DPB: $\zeta_{\omega x}$, $\zeta_{\omega y}$, and $\zeta_{\omega z}$. The experimental rotation times used to determine ζ_{rot} in the present work correspond to rotation of the long axis of the molecule (x), which can be related to these axis-specific constants by: $\zeta_{rot}^{-1} \cong \zeta_{\omega y}^{-1} + \zeta_{\omega z}^{-1}$. ($\zeta_{\omega y}$ and $\zeta_{\omega z}$ are the friction constants for motion *about* the y and z axes, which are the relevant motions for displacing a vector *along* the x axis.) The main result of importance here is that the simulations revealed considerable variation among different friction constants $\zeta_{\omega i}$, depending on the axis considered. At high densities in CO_2, one finds $\zeta_{\omega x}/\zeta_{rot} \approx 10$, $\zeta_{\omega y}/\zeta_{rot} \approx 3$, and $\zeta_{\omega z}/\zeta_{rot} \approx 1.5$. Without further calculations it is impossible to say how the reactive friction should be related to these rotational constants, but allowing for the likely possibility that $\omega_R^0/\omega_b^0 > 1$, the simulated values of $\zeta_{\omega i}/\zeta_{rot}$ suffice to indicate that the values of α found here are close to what one would anticipate for ζ/ζ_{rot}.

Whatever the value of ω_R^0/ω_b^0 is, if the present modeling is correct, the *relative* magnitudes of α should reflect significantly different relationships between reactive and rotational friction in the different solvent classes. Thus, if one assumes $\zeta \cong \zeta_{rot}$ in alkane solvents, these α values imply that ζ/ζ_{rot} is greatly reduced—by a factor of ~5 in alcohols and ~9 in perfluorinated solvents. Are such factors reasonable? Possibly. Recalling the 2−3-fold difference in C_{rot} between alcohol and alkane solvents and that C_{rot} itself varies by a factor of 2−3 in different *n*-alkanes, it seems at least plausible that the relationship between friction on rotation and reaction could vary by nearly an order of magnitude in different solvents. The fact that rotation senses the zero-frequency friction, whereas it is the friction at frequencies comparable to ω_b that is relevant for reaction, also lends credence to the possibility of significant variation among solvent types. Further computer simulations could be quite valuable in exploring this issue further.

IV. Summary and Conclusions

In this study we have measured the solvent dependence of emission characteristics, rotation times, and isomerization rates of diphenylbutadiene (DPB) in perfluoroalkane and alkane solvents. The low polarizabilities of the perfluoroalkane solvents facilitate the observation of systematic changes to the emission spectra and radiative rates of DPB, features of its photophysics which had previously gone unnoticed. These changes are ascribed to variations in the mixing between the $2A_g$ and $1B_u$ states as a function of solvent polarizability and potentially indicate a reversal of the state ordering at polarizabilities typical of perfluoroalkane solvents, as was recently suggested.[32]

The rotation times of DPB in nonpolar solvents depart significantly from the predictions of hydrodynamic models, but in a manner not quantitatively described by available molecular theories of rotational friction. A survey of literature data on comparable systems[7,65,82,100] shows that DPB is not unusual in this regard. Rather, these observations merely highlight the absence of any theory of rotational (or other) friction capable of quantitatively predicting the behavior of real solutes across a range of molecular solvents. In the absence of such a theory, the departures from hydrodynamic predictions can at least be correlated to simple solvent characteristics such as the ratio of solvent/solute size. We use such correlations to provide approximate values of rotational friction in cases where rotation data are not available.

With respect to the question originally motivating this study, do the "weak" interactions between aromatic hydrocarbons such as DPB and perfluorocarbon solvents lead to unusually weak frictional forces, the present rotation data (and data on translational diffusion[80]) appear to answer negatively. For a given pair of alkane and perfluoroalkane homologues (e.g., *n*-C_6H_{14} and *n*-C_6F_{14}) at a fixed value of η/T, rotation in the perfluorinated solvent is observed to be considerably faster than in its hydrogenated version. But this difference can be accounted for by the same size dependence of the rotational coupling factor that causes rotation times at fixed η/T to be smaller for large *n*-alkanes compared to those for small *n*-alkanes. In this regard, alcohol solvents, which are known to provide unexpectedly low friction on rotation of aromatic hydrocarbons,[82] appear more anomalous than do perfluorinated solvents.

The present study does not provide answers to a number of outstanding questions concerning the excited-state dynamics of DPB. The most important of these are: why is the isomerization yield lower than found in stilbene? and what role does the near degeneracy of the $2A_g$ and $1B_u$ states play in the excited-state dynamics? What we have observed is that the temperature- and solvent dependencies of the nonradiative decay rates of DPB in perfluoroalkane and alkane solvents do not depart in any noticeable way from what would be expected for an adiabatic process involving large-amplitude solute motion such as isomerization. We have therefore attempted to describe the measured rates in terms of Kramers' barrier crossing model in the spatial diffusion regime. To achieve a more meaningful fit to this model, we combined the data collected here with most of the previously reported data on DPB dynamics in alkane and alcohol solvents. Assuming that the friction on reactive motion is proportional to rotational friction, we fit all of these rate data to Kramers' theory[85] by adopting a model in which the reactive potential is a simple function of solvent dielectric properties. Such an approach proved moderately successful. Using a reactive potential constrained to match gas-phase data and assuming the barrier height to depend linearly on a dielectric field factor, we reasonably reproduced rate data encompassing a wide range of solvents and solvent conditions, but only after making one allowance for solvent individuality. To achieve acceptable fits requires that the proportionality between reactive

and rotational friction differs significantly among different solvent classes. Relative to the *n*-alkanes, proportionality constants of 0.7 in cyclic and branched alkanes, 0.1 in perfluoroalkanes, and 0.2 in *n*-alcohols are found. We note that the factor 0.1 here reflects a very modest solvent dependence of the reaction rate in perfluoroalkane solvents. Assuming that our modeling is correct, unlike the rotation data, the rate data indicate that reactive friction in perfluoroalkanes *is* unusually weak. It must be admitted, however, that in addition to reflecting real differences in the reactive friction in different solvent classes, these different coupling factors might also partially compensate for shortcomings in the potential model. Computer simulations of DPB in CO_2[8] suggest that it is not unreasonable to expect rotational and reactive friction to differ by as much as a factor of 10; however, whether the variations in this relationship among different solvent types is likely to be as large as implied by our modeling remains to be seen. The dramatic differences in rotational coupling in alcohol compared to that in alkane solvents (Figure 6) suggest that large variations with solvent might be expected. A more definitive answer should be available from computer simulations comparing various types of friction in different solvents. We are currently initiating such simulations.

Acknowledgment. We thank Zygmunt Gryczynski (Center for Fluorescence Spectroscopy, University of Maryland) and Richard Moog (Franklin and Marshall College) for making confirmatory quantum yield measurements, Donald Johnson for measuring the refractive indexes of the perfluoroalkanes examined here, and Jane Bogdanov for help with purification. This work was supported by funds from the Department of Energy Office of Basic Energy Science and from the National Science Foundation.

Supporting Information Available: Summary of collected data for DPB in nonpolar solvents (Table S-1). This information is available free of charge via the Internet at http://pubs.acs.org.

References and Notes

(1) Scott, R. *J. Phys. Chem.* **1958**, *62*, 136.
(2) Reed, T. M., III. Physical Chemistry of the Fluorocarbons. In *Fluorine Chemistry*; Simons, J. H., Ed.; Academic Press: New York, 1964; Vol. 5, p 133.
(3) Song, W.; Maroncelli, M.; Rossky, P. J. *J. Chem. Phys.*, in press, **2003**.
(4) Lawson, C. W.; Hirayama, F.; Lipsky, S. *J. Chem. Phys.* **1969**, *51*, 1590.
(5) Maciejewski, A. *J. Photochem. Photobiol., A* **1990**, *51*, 87.
(6) Maciejewski, A. *Chem. Phys. Lett.* **1989**, *163*, 81.
(7) Maroncelli, M. Unpublished results.
(8) Patel, N.; Biswas, R.; Maroncelli, M. *J. Phys. Chem. B* **2002**, *106*, 7096.
(9) Biswas, R.; Dahl, K.; Maroncelli, M. *J. Phys. Chem. B* **2002**, *106*, 11593.
(10) Velsko, S. P.; Fleming, G. R. *J. Chem. Phys.* **1982**, *76*, 3553.
(11) Keery, K. M.; Fleming, G. R. *Chem. Phys. Lett.* **1982**, *93*, 322.
(12) Courtney, S. H.; Fleming, G. R. *Chem. Phys. Lett.* **1984**, *103*, 443.
(13) Troe, J.; Amirav, A.; Jortner, J. *Chem. Phys. Lett.* **1985**, *115*, 245.
(14) Gehrke, C.; Schroeder, J.; Schwarzer, D.; Troe, J.; Voss, F. *J. Chem. Phys.* **1990**, *92*, 4805.
(15) Schroeder, J.; Schwarzer, D.; Troe, J. *Ber. Bunsen.-Ges. Phys. Chem.* **1990**, *94*, 1249.
(16) Gehrke, C.; Mohrschladt, R.; Schroeder, J.; Troe, J.; Vohringer, P. *Chem. Phys.* **1991**, *152*, 45.
(17) Mohrschladt, R.; Schroeder, J.; Schwarzer, D.; Troe, J.; Vohringer, P. *J. Chem. Phys.* **1994**, *101*, 7566.
(18) Schroeder, J.; Steinel, T.; Troe, J. *J. Phys. Chem. A* **2002**, *106*, 5510.
(19) Anderton, R. M.; Kauffman, J. F. *J. Phys. Chem.* **1994**, *98*, 12125.
(20) Anderton, R. M.; Kauffman, J. F. *J. Phys. Chem.* **1994**, *98*, 12117.
(21) Anderton, R. M.; Kauffman, J. F. *J. Phys. Chem.* **1995**, *99*, 13759.
(22) Anderton, R. M.; Kauffman, J. F. *J. Phys. Chem.* **1995**, *99*, 14628.
(23) Kauffman, J.; Wiemers, K.; Khajehpour, M. *Rev. High Pressure Sci. Technol.* **1998**, *7*, 1225.
(24) Lee, M.; Bain, A. J.; McCarthy, P. J.; Han, C. H.; Haseltine, J. N.; Smith, A. B., III; Hochstrasser, R. M. *J. Chem. Phys.* **1986**, *85*, 4341.
(25) Lee, M.; Haseltine, J. N.; Smith, A. B., III; Hochstrasser, R. M. *J. Am. Chem. Soc.* **1989**, *111*, 5044.
(26) Shepanski, J.; Keelan, B.; Zewail, A. *Chem. Phys. Lett.* **1983**, *103*, 9.
(27) Amirav, A.; Sonnenschein, M.; Jortner, J. *Chem. Phys.* **1986**, *102*, 305.
(28) Wallace-Williams, S. E.; Schwartz, B. J.; Moller, S.; Goldbeck, R. A.; Yee, W. A.; El-Bayoumi, M. A.; Kilger, D. S. *J. Phys. Chem.* **1994**, *98*, 60.
(29) Heimbrook, L.; Kohler, B.; Spiglanin, T. *Proc. Natl. Acad. Sci.* **1983**, *80*, 4580.
(30) Horwitz, J.; Kohler, B. E.; Spiglanin, T. *J. Chem. Phys.* **1985**, *83*, 2186.
(31) Itoh, T.; Kohler, B. *J. Phys. Chem.* **1988**, *92*, 1807.
(32) Itoh, T. *Chem. Phys. Lett.* **2001**, *342*, 550.
(33) Morris, D. L.; Gustafson, T. L. *J. Phys. Chem.* **1994**, *98*, 6725.
(34) Morris, D. L.; Gustafson, T. L. *Appl. Phys. B* **1994**, *59*, 389.
(35) Bachilo, S. M.; Spangler, C. W.; Gillbro, T. *Chem. Phys. Lett.* **1998**, *283*, 235.
(36) Saltiel, J.; Sun, Y.-P. Cis-Trans Isomerization of C═C Double Bonds. In *Photochromism*: *Molecules and Systems*; Dürr, H., Bouas-Laurent, H., Eds.; Elsevier: Amsterdam, 1990; p 64.
(37) Waldeck, D. H. *Chem. Rev.* **1991**, *91*, 415.
(38) Gorner, H.; Kuhn, H. J. *Adv. Photochem.* **1995**, *19*, 1.
(39) Allen, M.; Whitten, D. *Chem. Rev.* **1989**, *89*, 1691.
(40) Yee, W.; Hug, S.; Kliger, D. *J. Am. Chem. Soc.* **1988**, *110*, 2164.
(41) Eastman, L.; Zarnegar, B. M.; Butler, J. M.; Whitten, D. G. *J. Am. Chem. Soc.* **1974**, *96*, 2281.
(42) The $1B_u$ state in DPB and DPH are known to shift in a similar manner with solvent polarizability.[47]
(43) Rulliere, C.; Declemy, A.; Kottis, P. *Laser Chem.* **1985**, *5*, 185.
(44) Velapoldi, R. A.; Mielenz, K. D. *A Fluorescence Standard Reference Material*: *Quinine Sulfate Dihydrate*; NBS Special Publication 260-64; National Bureau of Standards: Washington, DC, 1980.
(45) Melhuish, W. H. *J. Phys. Chem.* **1961**, *65*, 229.
(46) Demas, J. N.; Crosby, G. A. *J. Phys. Chem.* **1971**, *75*, 991.
(47) Sklar, L. A.; Hudson, B. S.; Petersen, M.; Diamond, J. *Biochem.* **1977**, *16*, 813.
(48) Renge, I. *J. Photochem. Photobiol., A* **1992**, *69*, 135.
(49) If one measures frequencies in absorption and emission as ν_- and ν_+, the frequencies of the $^1/_2$ intensity points on the low- and high-frequency edges of the spectra, the differences between the absorption and emission shifts with solvent are much smaller, with the emission shifts generally being slightly larger than those in absorption.
(50) Wallace-Williams, S. E.; Moller, S.; Goldbeck, R. A.; Hanson, K. M.; Lewis, J. W.; Yee, W. A.; Kilger, D. S. *J. Phys. Chem.* **1993**, *97*, 9587.
(51) Moller, S.; Yee, W. A.; Goldbeck, R. A.; Wallace-Williams, S. E.; Lewis, J. W.; Klinger, D. S. *Chem. Phys. Lett.* **1995**, *243*, 579.
(52) Bunker, C. E.; Lytle, C. A.; Rollins, H. W.; Sun, Y.-P. *J. Phys. Chem. A* **1997**, *101*, 3214.
(53) Allen, M.; Miola, L.; Whitten, D. *J. Phys. Chem.* **1987**, *91*, 6099.
(54) Birch and Imhof[55] also reported the radiative rate of DPB in a methylcyclohexane + 2-methylpentane mixture and in propylene glycol to be 8.2×10^8 s^{-1}, approximately independent of temperature (−50 to +50 °C). Unfortunately, these measurements were based on assuming the quantum yield of the alkane mixture at 25 °C to be the same as the quantum yield of DPB in cyclohexane reported by Birks and Dyson.[59] Given the much larger viscosity of cyclohexane compared to the alkane mixture, this value is expected to substantially overestimate the radiative rate.
(55) Birch, D. J. S.; Imhof, R. E. *Chem. Phys. Lett.* **1982**, *88*, 243.
(56) Andrews, J.; Hudson, B. *J. Chem. Phys.* **1978**, *68*, 4587.
(57) Swofford, R. L.; McClain, W. B. *J. Chem. Phys.* **1973**, *59*, 5740.
(58) Fang, H. L.; Gustafson, T. L.; Swofford, R. L. *J. Chem. Phys.* **1983**, *78*, 1663.
(59) Birks, J. B.; Dyson, D. *Proc. R. Soc. London* **1963**, *A 275*, 135.
(60) For a detailed discussion on the friction on rotational motion of DPB see ref 8.
(61) The shape factor for stick boundary conditions was determined by numerically integrating the expressions in ref 62 and that for slip boundary conditions by interpolating the tabulated data in ref 63.
(62) Perrin, F. *J. Phys. Radium* **1934**, *5*, 497.
(63) Youngren, G. K.; Acrivos, A. *J. Chem. Phys.* **1975**, *63*, 3846.
(64) It is interesting to note that Hochstrasser and co-workers[25] had measured rotation times of the related solute "stiff-6 DPB" in the *n*-alkane series $n = 6-16$, and their times nearly coincide with the rotation times of DPB in *n*-alkanes shown in Figure 5.
(65) Horng, M.-L.; Gardecki, J.; Maroncelli, M. *J. Phys. Chem.* **1997**, *101*, 1030.
(66) Benzler, J.; Luther, K. *Chem. Phys. Lett.* **1997**, *279*, 333.

(67) De Backer, S.; Dutt, G. B.; Ameloot, M.; De Schryver, F. C.; Mullen, K.; Holtrup, F. *J. Phys. Chem.* **1996**, *100*, 512.

(68) Kim, S. K.; Fleming, G. R. *J. Phys. Chem.* **1988**, *92*, 2168.

(69) Zwanzig, R.; Harrison, A. K. *J. Chem. Phys.* **1985**, *83*, 5861.

(70) This expression provides an approximation to the 1/*e* times calculated for free rotors of various symmetries. I_{eff} is given by $I_{\text{eff}}^{-1} = I_1^{-1} + I_2^{-1}$ where I_1 and I_2 represent the two inertial moments that rotate the solute axis being observed.

(71) Spernol, V.; Wirtz, K. *Z. Naturforsch., A: Phys. Sci.* **1953**, *8*, 522.

(72) Gierer, A.; Wirtz, K. *Z. Naturforsch., A: Phys. Sci.* **1953**, *8*, 532.

(73) Dote, J. L.; Kivelson, D.; Schwartz, R. N. *J. Phys. Chem.* **1981**, *85*, 2169.

(74) If the sizes of solvent (v) and solute (u) molecules are measured in terms of volumes, defining the ratio $\rho \equiv (V_v/V_u)^{1/3}$, the Gierer−Wirtz[72] prediction can be written as

$$C_{\text{GW}}^{-1} = 6\rho\sum_{m=0}^{\infty}[1 + 2m\rho]^{-4}$$

Over the range of size ratios relevant here ($0.05 \le V_v/V_u \le 2$), one can use the more convenient form $C_{\text{GW}}^{-1} = 0.7746 + 5.313\rho^{1.10}$.

(75) The DKS predictions[73] can be expressed $C_{\text{DKS}}^{-1} = 1 + (\gamma/f_{\text{slip}})$ where $\gamma = (\Delta V_v/V_u)[4(V_u/V_v)^{2/3} + 1]$ and where ΔV_v is the volume of free space per solvent molecule. As recommended by Anderton and Kauffman,[20] we calculate ΔV_v from the difference between the molar and van der Waals volumes of the solvent, $\Delta V_v = V_m^v - V_{vdW}^v$.

(76) By defining a translational coupling constant in terms of departures from the Stokes−Einstein relation in the same manner as eq 5 for rotation, i.e., defining C_{trans} by $D_{\text{trans}}^{-1} = (6\pi r_u\eta/k_BT)C_{\text{trans}}$, the Spernol−Wirtz[71] prediction for the translational coupling factor can be written $C_{\text{SW}} = (0.16 + 0.4\rho^{-1})\{0.9 + 0.4T_r^v - 0.25T_r^u\}$, where ρ is the solvent/solute size ratio defined in 74, T_r^u and T_r^v are reduced solvent and solute temperatures, and $T_r^x = (T - T_{mp}^x)/(T_{bp}^x - T_{mp}^x)$ where T_{mp} and T_{bp} denote melting and boiling points, respectively. For the size ratio ρ here, we use the molar volume of the solvent and the van der Waals volume of toluene (the "translating" moiety, 98Å^3) after dividing the latter by $\chi = 0.74$, the packing fraction of close packed spheres.

(77) Sun, Y.-P.; Saltiel, J. *J. Phys. Chem.* **1989**, *93*, 8310.

(78) These volume ratios employ the molar volume of the solvent for V_v and the van der Waals volume of the DPB divided by a factor of 0.74, the packing fraction of close-packed spheres, $V_u = 167$ cm^3 mol^{-1}.

(79) In previous studies,[65] we have found that a similar function, but with the size ratio raised to a power, i.e., $C_{\text{rot}}^{-1} = 1 + a(V_v/V_u)^p$ with $p = 1.5$, provides a convenient representation of rotation data for a wide range of solutes and nonpolar solvents.

(80) Kowert, B.; Sobush, K. T.; Dang, N. C.; Seele, L. G.; Fuqua, C. F.; Mapes, C. L. *Chem. Phys. Lett.* **2002**, *353*, 95.

(81) Kowert, B. A.; Dang, N. C.; Sobush, K. T.; Steele, L. G., III. *J. Phys. Chem. A* **2001**, *105*, 1232.

(82) Williams, A. M.; Jiang, Y.; Ben-Amotz, D. *Chem. Phys.* **1994**, *180*, 119.

(83) In the course of fitting experimental data to the Kramers' model, we examined the effect of allowing for a single, temperature-independent contribution to k_{nr}. No significant improvement to the fits of *n*-alkane data was found using this extra parameter.

(84) The temperature dependence of the viscosity of the *n*-alkanes and the perfluoro-*n*-alkanes over the range $n = 6-9$ can be well represented by the function: $\ln(\eta/\text{cP}) = A(n) + (\Delta H_\eta(n)/RT)$ with $A(n) = -3.436 - 0.108n$ and $\Delta H_\eta(n)/\text{kJ mol}^{-1} = 1.193 + 0.974n$ in the case of the *n*-alkanes and $A(n) = -2.807 - 0.339n$ and $\Delta H_\eta(n)/\text{kJ mol}^{-1} = 0.743 + 1.706n$ for the perfluoro-*n*-alkanes. (Based on fits to data from ref 102 in the case of the alkanes and refs 2, 103, and 104 in the case of the perfluoroalkanes.)

(85) Kramers, H. A. *Physica* **1940**, *7*, 284.

(86) Berne, B. J.; Borkovec, M.; Straub, J. E. *J. Phys. Chem.* **1988**, *92*, 3711.

(87) Fleming, G. R.; Hanggi, P. *Activated Barrier Crossing*; World Scientific: Singapore, 1993.

(88) Pollak, E. Theory of Activated Rate Processes. In *Dynamics of Molecules and Chemical Reactions*; Wyatt, R., Zhang, J., Eds.; Marcel Dekker: New York, 1996; p 617.

(89) Hanggi, P.; Talkner, P. *Rev. Mod. Phys.* **1990**, *62*, 251.

(90) We also examined use of a quadratic function but the added flexibility did not provide substantially better results.

(91) Excluded from this fitting are the room-temperature *n*-butane data from ref 14 which appear to be anomalous relative to the other data in that work.

(92) $\chi_\nu^2 \equiv (1/\nu)\sum_i(y_i - y_i^{\text{fit}})^2/\sigma_i^2$ where ν is the number of degrees of freedom in the sample, y_i and σ_i are the observed value and uncertainty in data point *i*, and y_i^{fit} is the fitted value of this point.[93]

(93) Bevington, P. R. *Data Reduction and Error Analysis for the Physical Sciences*; McGraw-Hill: New York, 1969.

(94) Rotation times were derived from the τ_{rot} versus η/T parametrizations listed in Table 3 of ref 20 by using parametrizations of $\eta(T)$ in *n*-alcohols tabulated in ref 107. Nonradiative rates were read from the lines in Figure 2 of ref 19 (which disagreed slightly with values determined from the parametrizations of Table 1 of that paper.) These nonradiative rates were recalculated to incorporate our $k_{\text{rad}}(n)$ dependence; however, because $k_{\text{nr}} >> k_{\text{rad}}$ in the alcohols, the values were little changed from those originally reported. Values of dielectric parameters ϵ and n_D were obtained from the parametrizations in ref 101.

(95) The values of rotational friction calculated by Anderton and Kauffman in ref 19 are approximately 2-fold smaller than the ones calculated here because of a missing factor of two in the effective moment of inertia used by those authors.

(96) Some part of this deviation may be due to experimental uncertainties beyond those we have assigned to the data. The atmospheric pressure data from ref 17 (methanol−pentanol) differ from those in ref 19 by 18−41%. For this reason, we have adopted larger values of the uncertainties when fitting the alcohol data: ±10% in k_{obs} (±20% when $\tau_{\text{obs}} < 50$ ps, the resolution of the instrument used in ref 19). We also note that in the case of methanol, the data in ref 17 are 20% smaller than those from ref 19 and are therefore in much closer agreement with the predictions of the fit.

(97) Khajehpour, M.; Kauffman, J. *J. Phys. Chem. A*, **2000**, *104*, 9512.

(98) Reynolds, L.; Gardecki, J. A.; Frankland, S. J. V.; Horng, M. L.; Maroncelli, M. *J. Phys. Chem.* **1996**, *100*, 10337.

(99) Equation 19 is slightly nonstandard in that solvation energies dipolar solutes are typically written in terms of the reaction field factor $f_2(\epsilon) = 2(\epsilon - 1)/(2\epsilon + 1)$, rather than $f(\epsilon) = (\epsilon - 1)/(\epsilon + 2)$. Equation 19 can be derived as follows. The free energy of solvation of polarizable point dipole with gas-phase moment μ and polarizability α in a spherical cavity of radius *a* can be written:[108] $G = -(\mu^2/2a^3)(f_2(\epsilon)/[1 - (\alpha/a^3)f_2(\epsilon)]$. A survey of molecules shows that typical values of α/a^3 are 0.3−0.6.[109] Assuming a value of $(\alpha/a^3) = (1/2)$ leads to eq 19. We have examined fits using the above more general equation with a range of values of α/a^3 and find no significant difference in the quality of the fits compared to those using eq 19.

(100) Ravi, R.; Ben-Amotz, D. *Chem. Phys.* **1994**, *183*, 385.

(101) Marcus, Y. *The Properties of Solvents*; Wiley: New York, 1998.

(102) Frenkel, M. *TRC Thermodynamic Tables−Hydrocarbons*; National Institute of Standards and Technology: Gaithersburg, MD, 2002.

(103) *Landolt−Börnstein*: *Numerical Data and Functional Relationships in Science and Technology*; Springer-Verlag: New York, 1974; Vol. II/6.

(104) Haszeldine, R.; Smith, F. *J. Chem. Soc.* **1951**, *1951*, 603.

(105) Wiemers, K.; Kauffman, J. F. *J. Phys. Chem. A* **2000**, *104*, 451.

(106) Chattopadhyay, S.; Das, P.; Hug, G. *J. Am. Chem. Soc.* **1982**, *104*, 4507.

(107) Yaws, C. L. *Handbook of Viscosity*; Gulf Publishing Co.: Houston, 1995; Vol. 1−3.

(108) Bottcher, C. J. F.; Bordewijk, P. *Theory of Electric Polarization*, 78th ed.; Elsevier: Amsterdam, 1978; Vol. II.

(109) Kumar, P. V.; Maroncelli, M. *J. Chem. Phys.* **1995**, *103*, 3038.